UNIVERSIDADE D
COIMBRA

Miguel Caridade Gaspar

OPTIMAL INSTALLATION AND USE OF SENSOR SYSTEMS ON AUTONOMOUS VEHICLES FOR ROUGH TERRAIN

Dissertação no âmbito do Mestrado Integrado em Engenharia Mecânica na área de Produção e Projeto, orientada pelo Professor Doutor Carlos Xavier Pais Viegas, coorientada pelo Professor Doutor Pedro Mariano Simões Neto e apresentada ao Departamento de Engenharia Mecânica da Faculdade de Ciências e Tecnologia da Universidade de Coimbra.

Julho de 2022

1 2 9 0

FACULDADE DE CIÊNCIAS E TECNOLOGIA
UNIVERSIDADE D COIMBRA

Optimal installation and use of sensor systems on autonomous vehicles for rough terrain

Submitted in Partial Fulfilment of the Requirements for the Degree of Master in Mechanical Engineering in the speciality of Production and Project

Otimização da instalação e uso de sistemas de sensores em veículos autónomos para terrenos acidentados

Author

Miguel Caridade Gaspar

Advisors

Prof. Dr. Carlos Xavier Pais Viegas

Prof. Dr. Pedro Mariano Simões Neto

Jury

President	Professor Doutor **Miguel Rosa Oliveira Panão** Professor Auxiliar da Universidade de Coimbra
Vowels	Professor Doutor **Ricardo Nuno Madeira Soares Branco** Professor Auxiliar da Universidade de Coimbra
	Professora Doutora **Trayana Stoykova Tankova** Professora Auxiliar da Universidade de Coimbra
Advisor	Professor Doutor **Carlos Xavier Pais Viegas** Professor Auxiliar da Universidade de Coimbra

Institutional Collaboration

Association for the Development of Industrial Aerodynamics

Coimbra, July, 2022

ACKNOWLEDGEMENTS

This thesis would not be possible without the support and contributions of those who in many and different ways lent a helping hand during its development. My deepest gratitude goes to everyone who in some way heightened the work here presented.

To my advisor, Professor Doctor Carlos Xavier Pais Viegas, for his continued availability throughout this work, for all the help and support given in every step, and for the opportunity to contribute to the work developed by his team.

To my co-advisor, Professor Doctor Pedro Mariano Simões Neto, for his availability throughout this work.

To the Field Tech Laboratory team, Babak Chehreh, Diogo Valério, Ricardo Baila, Tiago Gameiro and Tiago Pereira, for their friendship and their time, and for their invaluable contributions to this dissertation.

To my family, for their affection and for always looking out for me, be it from near or from afar.

To my parents, Milú and Joaquim, for being a constant presence in my life, for supporting me in everything I do, for giving me all the tools needed to succeed and always being available to help, and for their love.

To my brother, Tomás, and to Lu, for never failing to make me laugh and for making life better.

And to Carolina, for always motivating me to do my best, for always being there, for making the bad days easier and the good days better, and for her patience, love and kindness.

Abstract

In today's context, the automation of tasks and processes is continuously expanding, as harsh environments, shortages of manual labour and constant technological developments create a world where machines thrive. However, the process of automating an already existing machine is still a largely underdeveloped domain.

In forestry robotics, more specifically in wildfire combat, remote controlled mulching machines are oftentimes used for land clearing operations, as fuelbreak management is an efficient fire prevention method. But these machines require the presence of on-site personnel, thus limiting their potential effectiveness.

The current work looks to contribute to the development of an autonomous robotic platform for fuelbreak management, focusing on the integration of sensors on the machine, aiming to optimise sensor performance. The final goal of this thesis is the elaboration of a series of guidelines for the installation of sensory systems in any machine inside the scope of field robotics.

The work starts with the research of the current state-of-the-art on autonomous robots and the effect of different characteristics on sensor performance, namely mounting location, temperature, dust, vibrations, ambient light, and rain. Tests were carried out to assess the impact of these different constraints on the introduced robotic platform, and all conducted tests are presented and discussed.

The results and conclusions garnered allowed the elaboration of a set of guidelines for the installation of complete sensory systems in field robotics applications looking to automate their operations. The work is also believed to have contributed to guiding the installation of individual sensors on any machine, for operation in a multitude of differently constrained environments.

Keywords: Autonomous robots, Robust sensory systems, Field robotics, Forest navigation, Sensor integration guidelines, Outdoor environments.

Resumo

No contexto atual, a automatização de tarefas e processos está continuamente em expansão, dado que ambientes severos, a escassez de trabalho manual e os constantes desenvolvimentos tecnológicos criam um mundo onde as máquinas prosperam. No entanto, o processo de automatização de uma máquina já existente é um campo ainda subdesenvolvido.

Em robótica florestal, mais especificamente no combate a incêndios florestais, as máquinas destroçadoras controladas à distância são frequentemente utilizadas para operações de limpeza de terrenos, uma vez que a criação de faixas de gestão de combustível é um método eficiente na prevenção de incêndios. Mas estas máquinas requerem a presença de pessoal no local, limitando assim a sua potencial eficácia.

Esta dissertação procura contribuir para o desenvolvimento de um robô autónomo para a criação e manutenção de faixas de gestão de combustível, dando especial atenção à integração de sensores na máquina, visando a otimização do desempenho dos sensores. O objetivo final desta tese é a elaboração de uma série de diretrizes para a instalação de sistemas sensoriais em qualquer máquina dentro do domínio da robótica de campo.

O trabalho começa com a investigação do atual estado da arte sobre robôs autónomos e o efeito de diferentes condições no desempenho dos sensores, nomeadamente local de instalação, temperatura, poeira, vibrações, luz ambiente, e chuva. Foram realizados testes para avaliar o impacto destas diferentes condições na plataforma robótica introduzida e todos os testes realizados são apresentados e discutidos.

Os resultados e conclusões obtidas permitiram a elaboração de um conjunto de diretrizes para a instalação de sistemas sensoriais em aplicações robóticas de campo, com vista a automatizar as suas operações. Acredita-se também que o trabalho contribuiu para orientar a instalação de sensores individuais em qualquer máquina, para operação em múltiplos ambientes com características diferentes.

Palavras-chave: Robôs autónomos, Sistemas sensoriais robustos, Robótica de campo, Navegação florestal, Diretrizes para integração de sensores, Ambientes exteriores.

CONTENTS

LIST OF FIGURES

LIST OF TABLES

LIST OF ACRONYMS AND ABBREVIATIONS

3D – Three-Dimensional

AI – Artificial Intelligence

CAD – Computer Aided Design

CMOS – Complementary Metal Oxide Semiconductor

DoF – Degrees of Freedom

EO – Electro-Optical

FFT – Fast Fourier Transform

GNSS – Global Navigation Satellite Systems

GPS – Global Positioning System

ICE – Internal Combustion Engine

IMU – Inertial Measurement Unit

IR – Infrared

LeGo-LOAM – Lightweight and Ground-Optimized LiDAR Odometry and Mapping

LiDAR – Light Detection and Ranging

LWIR – Long-Wave Infrared

MR – Magnetorheological

RGB – Red, Green, and Blue

RPM – Revolutions Per Minute

RTK – Real Time Kinematics

SLOAM – Semantic LiDAR Odometry and Mapping

TIR – Thermal Infrared

TMD – Tuned Mass Damper

TOPS – Trillion Operations Per Second

UAV – Unmanned Aerial Vehicles

UGV – Unmanned Ground Vehicle

VD – Variable Damping

VS – Variable Stiffness

WRI(s) – Wire Rope Isolator(s)

1. INTRODUCTION

Every year, wildfires rage across Portugal and the world, drastically changing ecosystems, polluting the air, destroying homes, and claiming human lives. Between the years of 2000 and 2021, a cumulative area of nearly 3 million hectares burned in Portugal (see Figure 1.1), with many regions suffering from several re-burn scenarios. In 2017 alone, a series of fire events were started in or close to the municipality of Pedrógão Grande, eventually leading to the deaths of 65 people and burning over 45 thousand hectares [1].

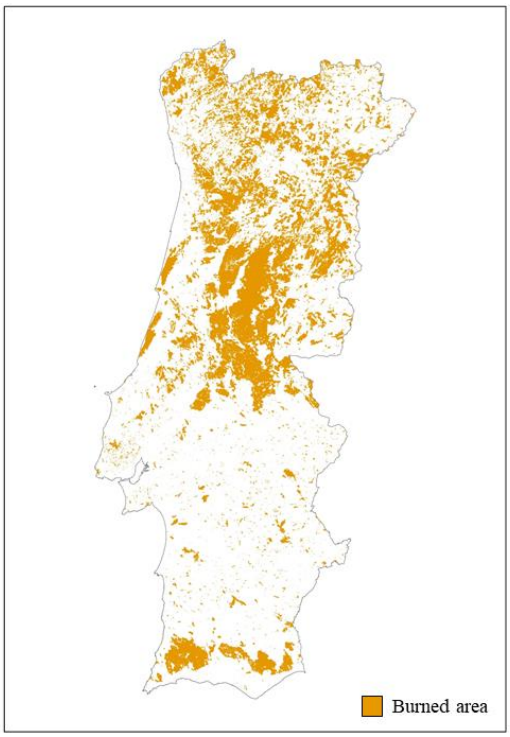

Figure 1.1 - Cumulative burned area in Portugal between 2000 and 2021, compiled with information from [2]

Given the devastating effects of wildfires, and the many times fatal aftermaths of firefighting, fire prevention methods offer safer alternatives for wildfire combat. A way of hampering fire propagation is through the limitation of the biomass available for combustion, which can be achieved with the creation of firebreaks and fuelbreaks.

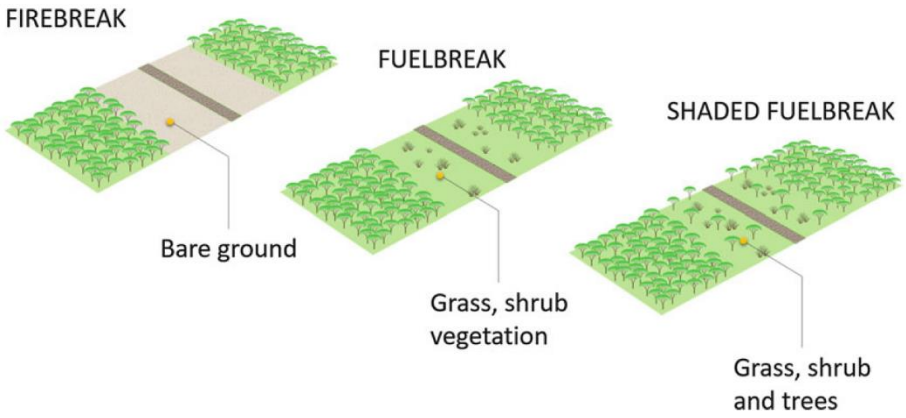

Figure 1.2 - Differences between firebreaks, fuelbreaks and shaded fuelbreaks, retrieved from [3]

Fuelbreak is a linear path in which any fuel source, ranging from surface fuel to canopy fuel, has been reduced or modified to diminish the risk of the spread of fire crossing said path. The creation and maintenance of fuelbreak networks often occurs in remote and demanding environments, making it an arduous and dangerous work, furthermore, the pandemic currently affecting most of the world made clear that very few tasks can be completed without an on-site human presence, at least not with the same effectiveness. Ergo, it is only natural that new and innovative solutions are designed to either allow remote operations to be conducted or to further the development of fully autonomous alternatives.

The current thesis presents the development of an autonomous robotic platform for fuelbreak management and land clearing operations, focusing primarily on the integration of sensory systems.

This research work is partially funded by the projects rePlant – Implantação de estratégias colaborativas para a gestão integrada da floresta e do fogo (POCI-01-0247-FEDER-046081), F4F – Forest for Future (CENTRO-08-5864-FSE-000031) and E-Forest – Framework multi-agente de plataformas robóticas autónomas de propulsão elétrica para a gestão da floresta (POCI-01-0247-FEDER-047104).

In the current chapter, the motivations behind the work are discussed, mainly through the optic of wildfire prevention and how automation can benefit this field. Then, the objectives of this thesis are explored, also showing the need for better guidelines concerning the installation of sensory systems on machines, followed by a presentation of the robotic platform in which the work will be conducted, predominantly focusing on the machine and sensors to be used. Finally, the outline of the dissertation, with a brief description of each chapter, is introduced.

Figure 1.3 - Funding projects logos

1.1. Motivation

Firefighting begins long before the start of an actual fire. Fire prevention is the main strategy by which wildfires can be fought without the need for direct contact with the fire, thus limiting firefighters' exposure to danger and possible death. Fire prevention through the method of fuel treatment (i.e., reducing the biomass available for combustion) can be achieved by numerous techniques, including pruning, grazing, thinning and prescribed burning.

Whereas pruning and grazing are more easily applied to smaller, more contained areas [4], forest thinning, and prescribed burnings can facilitate fuel management in bigger forests. Prescribed burning is the planned and controlled use of fire aimed at reducing fuel loads to minimize the size or incidence of wildfires, the practice, however, is risky because prescribed burns can and do sometimes escape control and result in heavy smoke and damaging wildfires [5].

Thinning, on the other hand, does not involve the use of fire and, as such, does not carry the associated risks. Thinning techniques easily reduce the amount of flammable vegetation, thus enabling the creation of fuelbreaks. However, manual forest thinning is often a hazardous work requiring a considerable workforce, which in turn is expensive; therefore, the capability of automating thinning processes can safeguard workers while reducing operating costs and increasing overall efficiency.

Regarding forestry applications, not many solutions exist where an autonomous robot is used for purposes other than observation and data collection, which is to say most vegetation removal machines are dependent on either direct manual operation or the presence of an on-site operator for remote control. Shortages of manual labour then heavily diminish the amount of work that can be achieved, so a need for autonomous systems arises.

From a broader perspective, the lack of standards and guidelines for the installation of sensory systems in robotic applications often leads to a trial and error approach when selecting and mounting sensors onto the machine. This absence of guidelines, created by the inexistence of scientific works that relate sensor mounting solutions to sensor performance,

paired with the few existing examples of automation in forest cleaning applications, prompt the need for the work developed in this thesis.

1.2. Goals

The primary goals of this work are to study the correlation between sensor mounting locations and sensor performance, and to evaluate the effect of different internal and external constraints on sensor performance. The work will be developed in a specific platform, a diesel-powered mulching machine, aiming to optimise both sensor use and location to enable its automation in field robotics applications, namely vegetation removal in unstructured terrain.

Therefore, to decide and validate each sensor's installation method, several steps must be carried out:

- Understanding of the chosen sensors;
- Testing of different solutions for sensor mounting in the specified platform, focusing on performance in the forestry application considered;
- Assessment of the impact of vibrations on sensor performance and testing of different vibration damping alternatives to reduce measurement noise;
- Assessment of the impact of different environment conditions in each individual sensor;
- Performance evaluation of the complete sensory system in different environment conditions;
- Determination of the optimal setup for the specific platform tested.

The final goal of the present dissertation is the elaboration of a series of recommendations or guidelines for the installation of sensory systems with the purpose of facilitating automation, applicable to any machine inside the scope of field robotics.

1.3. Robotic platform

In this subchapter, the robotic platform in which the work will be conducted is detailed, introducing the machine used for the task of forest cleaning, the control module to be used, and the set of sensors to be installed on the machine, which, when connected to the control module, will allow the platform to function autonomously.

1.3.1. The machine

The machine to be adapted for sensor mounting is the Green Climber LV400 Pro model, developed by MDB Technologies [6], which can be observed in Figure 1.4. It is a heavy-duty, remote controlled device, powered by a 3 cylinder, water cooled, internal combustion diesel engine with 26.9 kW.

Figure 1.4 - The Green Climber LV400 Pro

Through the use of an extendable undercarriage (see Figure 1.5), increasing its width from 1170 to 1570 mm, the LV400 can adapt its grip on the terrain, allowing it to drive over slopes with gradients of up to 60° in any direction. The machine also has interchangeable attachments, allowing its use in a multitude of applications, ranging from its primary usage for mulching and land clearing to wood chipping, tree spraying and even snow blowing.

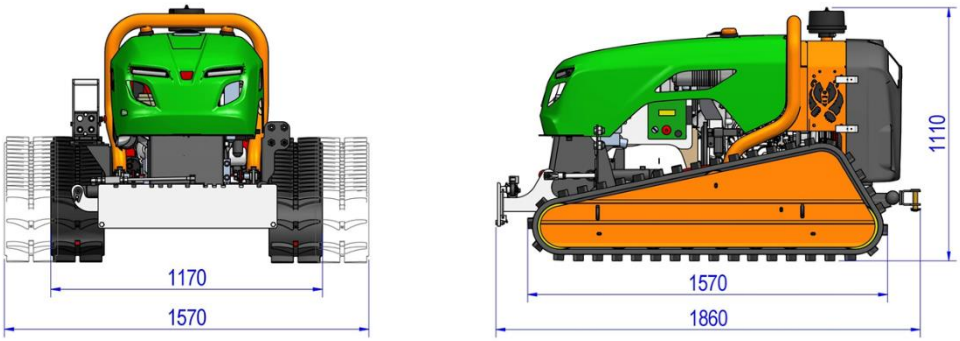

Figure 1.5 - Front and side view of the Green Climber LV400 Pro without attachments, with dimensions, retrieved from [7]

The machine's control unit will be a NVIDIA Jetson Xavier NX, a compact module used for multi-modal AI (Artificial Intelligence) applications. Capable of delivering up to

21 TOPS (Trillion Operation Per Second), according to NVIDIA [8], this control unit proves ideal to process high resolution data from multiple sensors simultaneously.

1.3.2. The sensors

Several sensors will be installed on the robot and will send their respective data to the Jetson Xavier NX control unit, which will then compile all the received information and output commands for the machine actuators, with the aim of allowing it to function autonomously.

- LiDAR sensor:

Puck™ (previously VLP-16), a LiDAR (Light Detection and Ranging) sensor, developed by Velodyne Lidar, with a 360° surrounding horizontal field of view and a 30° vertical field of view. The Puck has a wavelength of 905 nm and a range of 100 m, which allows the generation of up to 600,000 points per second. It also has an IP67 rating, which makes it dust-tight and protected against powerful water jets [9].

According to Ullrich [10], the main metrics for assessing the quality of LiDAR measurements are nominal sampling frequency, measured in points per metre, which is the inverse of the more traditionally used metric of nominal point spacing (NPS); and nominal point density, measured in points per square metre, which translates to the number of points within some test region, divided by the area of that region.

- RGB + Depth camera:

Intel® RealSense™ D435i, a depth camera that uses stereo vision to calculate depth. Depth video streams are like colour video streams, except each pixel has a value representing the distance away from the camera instead of colour information, even so, the camera still includes a RGB colour sensor that allows for colour data to be registered. The D435i also includes a 6 Degrees of Freedom (6DoF) IMU (Inertial Measurement Unit), especially effective in situations where the camera is subjected to movement. According to its data panel, the sensor has a range from 0.2 m to over 10 m and a diagonal field of view of over 90°.

- GNSS + RTK + IMU:

Duro Inertial, an enclosed dual-frequency GNSS (Global Navigation Satellite Systems) receiver with an integrated inertial navigation system, developed by Swift Navigation. The Duro Inertial combines standard GNSS with RTK (Real Time Kinematics)

technology to improve accuracy, allowing for centimetre-accurate positioning. The cast aluminium housing is rated for IP67, making it ideal for outdoor, harsh environments.

The 6DoF IMU, a Bosch BMI160, integrated on the Duro Inertial, allows for accelerometer and gyroscope measurements to be taken, enabling even more accurate positioning in challenging GNSS / RTK contexts, as the vehicle state can be more precisely estimated by fusing IMU measurements and GNSS data.

- IR camera:

FLIR ADK, a thermal infrared (IR) camera with a thermal sensitivity of under 50 mK and a horizontal field of view of 75°, measures the LWIR spectral band (Long-Wave Infrared) with wavelengths between 8 and 14 µm. Created by Teledyne FLIR, the camera is also IP67-rated and is able to operate in any weather condition, in part due to the incorporation of a heated external window.

For TIR (thermal infrared) cameras, surface emissivity has a very strong impact on the magnitude of the measurement error [11]. In forest environments, it is of paramount importance to accurately estimate the surface emissivity of the vegetation to be measured, so that corrective steps can be taken to reduce the expected errors.

Likewise, the angle of view strongly affects the measurements of thermal infrared cameras. In [12], it was determined that for angles of view of over 50° IR measurements start to gain considerable errors, with the error magnitude rapidly increasing when the angle of view increases past the 50° mark.

- Multispectral camera:

Genie Nano-CL C2420, a multispectral camera capable of capturing both the visible spectrum (400 to 700 nm) and the near infrared spectrum (700 to 1000 nm). Developed by Teledyne DALSA, the Genie Nano uses a range of CMOS (complementary metal oxide semiconductor) image sensors, allowing for higher resolutions, while still maintaining a robust build quality due to its IP30-rated enclosure.

The use of a multispectral camera also allows for the separation of the RGB channel into individual red, green and blue ones, which enable the creation of false colour images where specific features can be enhanced.

1.4. Outline

The ensuing chapters in this dissertation present the remainder of the work conducted. In the next chapter, the relevant state-of-the-art in forestry robotics is introduced, namely the main challenges tied to forest navigation, some examples of existing robots designed for forestry applications, and the notable constraints that make the installation of sensors on this type of machines difficult.

The third chapter details the work developed, together with the methodologies followed in each experimental test. Then, the fourth chapter delineates the recommended requirements for the installation of each sensor based on the results obtained, while also introducing a set of guidelines that can be applied to the broader domain of field robotics.

The fifth and final chapter presents the conclusions of the thesis, summarising the results obtained and the challenges that arose during the progression of the work, along with the possible opportunities for development in the future to heighten the already completed work.

2. STATE-OF-THE-ART

The current state-of-the-art in forestry robotics is predominantly aimed at the development of flora identification and forest monitoring robots and not combustible material removal machines, as such, not many solutions exist where an autonomous robot is used for other than observation and data collections purposes. Most vegetation removal machines are dependent on either a direct hands-on operation, such as the 125VRT Mulching Tractor developed by Fecon [13], or a remote-control operation, such as the Green Climber division developed by MDB Technologies [14].

In this section, a brief introduction to the specific challenges tied to forest navigation is made, followed by a presentation of several examples of robots designed for forestry applications and their characteristics, with emphasis on the types of sensors used. The third subsection addresses the prevalent techniques in the field of vibration damping and which strategies are better suited to reduce vibrations that could affect sensors on mobile vehicles. In the fourth subsection the problems tied to dust and other particulates are introduced, while the fifth subsection explores the influence of the amount of light on sensor accuracy. Lastly, a summary of how each effect affects each sensor is shown.

2.1. Challenges of forest navigation

As detailed in [15] there are only a small number of robots developed for forestry applications, mainly due to the complex nature of forest environments, which makes the development of robust robots difficult.

Notable challenges in developing robots for forest applications are:

- Unstructured environment – the lack of clear paths and the presence of steep slopes along with stony elements and other obstacles translate into a need for reliable localization and navigation systems [16], [17]
- Lack of GPS (Global Positioning System) accuracy – most times, the presence of trees and thick vegetation makes the use of GPS systems for localization and navigation impractical [18], ergo different solutions are needed in order to allow safe and accurate navigation [19]

- Locomotion systems – given the complex nature of forest environments not all locomotion systems are ideal, or even feasible, for forestry applications [20]
- Changes in ambient light, humidity and temperature – changes in the surrounding environment can lead to situations where certain sensors have reduced accuracy or are simply incapable of working, as such, these constraints must be taken into account when selecting the sensors to be used.
- Vibrations, either due to the robot's internal components, like the engine, or due to external elements, such as travelling in unstructured terrain – vibrations can cause sensors to lose effectiveness, which can prove detrimental to the robot's capabilities.
- Dust and other particulates – like vibrations, dust or other particulates, such as smoke, rain and water vapour, can cause sensors to be unable to complete the necessary task, namely sensors that rely on cameras or light, such as the LiDAR, the stereo depth camera, or the multispectral camera.

2.2. Examples of robots and types of sensors used

Given the similarities involved, both firefighting and agricultural robots present excellent opportunities to draw parallels between these types of applications and forest cleaning robots, the first two subsections are dedicated to the presentation of robots developed to fulfil these applications.

On robots designed specifically for forestry applications a distinction can be made between observation and data collection robots and forest cleaning robots, as such, both types of robots have a specific subsection where different existing solutions are presented.

2.2.1. Firefighting robots

Firefighting robots (Figure 2.1) originate from the need to help firefighters combat wildfires (or any other type of fires), their main objective is to allow faster and more efficient water spraying. Their leading characteristics are resistance to high temperature environments, the capacity to navigate rough and unstructured terrains, normally saturated with smoke and gases, and the ability to store great quantities of water or necessary equipment.

(a) (b) (c)

Figure 2.1 - Examples of robots used in firefighting scenarios: (a) Colossus [21], (b) Multiscope Rescue with Hydra [22], (c) Fire Ox [23]

The Colossus robot [21] was announced by the French company Shark Robotics in 2017. It is a modular robot, which allows it to assist in different scenarios, most notably, the robot can be equipped with a water cannon capable of delivering 3000 L/min. Due to its tracks locomotion system, the Colossus is able to drive over challenging terrain, as well as climb stairs. The chassis, made of aluminium-welded aeronautical steel, gives the robot waterproofing and heat resistance up to 900 °C. In order to allow remote control, it is equipped with a motorized pan-tilt-zoom camera and a thermal camera. Optionally, the Colossus can be integrated with chemical, biological, radiological, and nuclear sensors, so as to expand its applications.

Multiscope Rescue with Hydra [22] is a firefighting robot developed by Milrem Robotics. Designed to be used for industrial, warehouse, tunnel and wildfire extinguishing, the robot helps to combat fires in dangerous or difficult to access areas.

Developed by Lockheed Martin and BFX Fire Apparatus, the Fire Ox [23] is a six-wheel drive military autonomous land vehicle adapted to perform firefighting operations. The robot can be remote controlled with the help of RGB cameras and allows for day and night non-line-of-sight operation as well as hot spot detection through Infrared (IR) and Electro-optical (EO) cameras.

A common characteristic across all three robots is that all cameras are mounted in high locations with unobstructed fields of view to allow maximum observation capabilities, whereas the other sensors are installed in more interior and protected locations.

Table 2.1 summarizes the locomotion systems and sensors used by each robot mentioned in this subsection.

Table 2.1 - Comparison of the analysed firefighting robots

Robot	Locomotion System	Sensors Used
Colossus [21]	Tracks	GPS, RGB camera, Infrared camera, IMU, Extra sensors
Multiscope Rescue with Hydra [22]	Tracks	RGB camera, Infrared camera
Fire Ox [23]	Six-Wheel Drive	RGB camera, Infrared camera, Electro-optical camera

2.2.2. Agricultural robots

Agricultural robots (Figure 2.2) arise from the increasing demand for food production for an ever-growing world population. The ability to automate agricultural processes, such as planting, harvesting, sowing, and spraying, allows for more efficient processes, which in turn lead to faster production rates.

(a) (b)

Figure 2.2 - Examples of robots used in agricultural applications: (a) PowerBlast 500 Gallon tree sprayer [24], (b) Vegebot [25]

Partel et al. [24] developed an automated tree crop sprayer by adding several sensors to a PowerBlast tree sprayer, thus creating a smart sensing system capable of controlling airblast spray applications. The prototype used LiDAR, GPS and RGB cameras in order to determine tree height, tree classification and fruit count. The developed system led to a 28% reduction in spraying volume compared to the conventional method of constant spraying.

The Vegebot robot [25] was developed for lettuce harvesting, the robot employs two RGB cameras capable of identifying lettuce heads and then proceed with their removal. A control method was developed to monitor the force applied during the harvesting process, so as to not damage the vegetables.

Table 2.2 summarizes the locomotion systems and sensors used by each robot mentioned in this subsection.

Table 2.2 - Comparison of the analysed agricultural robots

Robot	Locomotion System	Sensors Used
Smart tree crop sprayer [24]	2 Wheels (pulled with tractor)	GPS, LiDAR, RGB cameras
Vegebot [25]	4 Wheel Drive	RGB cameras

2.2.3. Observation and data collection robots

Several advances have been made in the development of solutions capable of collecting data from forests, especially in the UAV (Unmanned Aerial Vehicles) field, where multiple applications exist with the sole purpose of monitoring the state of forests, leading to better fire prevention networks.

Observation and data collection robots (Figure 2.3) allow forest monitoring to be conducted remotely or even automatically and, apart from improving fire detection systems, can also be applied to monitoring the state of infrastructure existent in forests.

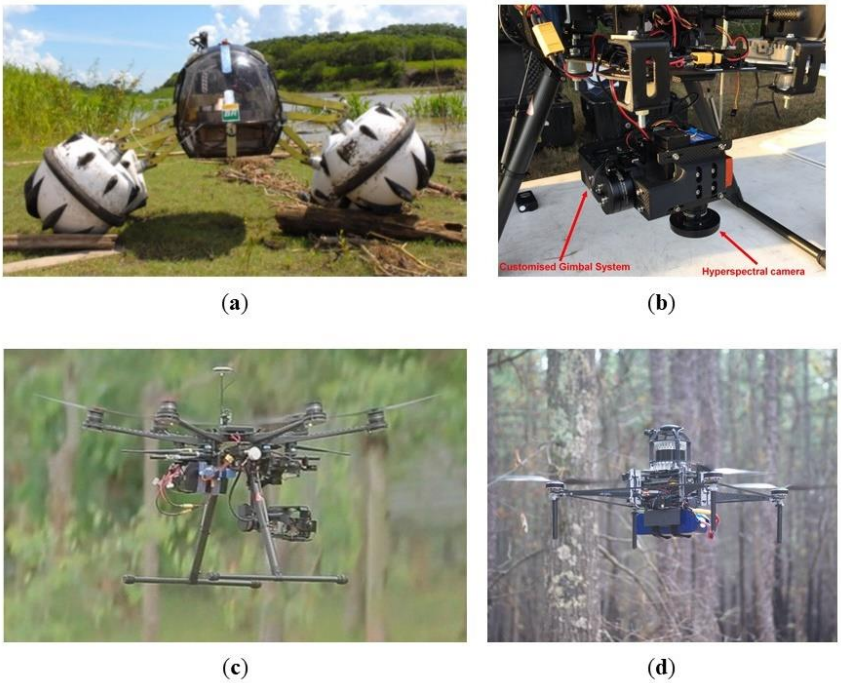

Figure 2.3 - Examples of robots used in forestry data collection applications: (a) Environmental Hybrid Robot [26], (b) UAV robot 1 [27], (c) UAV robot 2 [28], (d) UAV robot 3 [29]

One of such examples is the Environmental Hybrid Robot [26], designed to operate in the Amazon rainforest to conduct monitoring missions for a Brazilian oil company. The robot, equipped with several sensors to check for possible gas leaks and water pollution, has

a wheel-legged locomotion system with active reconfiguration that allows it to travel over rough terrain, sand, swamps and even water.

However, most robots designed for observation fall under the UAV category – flight-based systems capable of collecting data from an aerial vantage point, thus allowing the coverage of bigger areas whilst eliminating the need for obstacle avoidance. Sandino et al. [27] utilised hyperspectral sensors installed on an UAV, combined with machine learning algorithms, to conduct aerial mapping of forest affected by pathogens. In [28], an UAV was equipped with GPS, an Inertial Measurement Unit (IMU) and thermal and RGB cameras and then used to monitor koala activities in order to help their preservation. And in [29], an UAV was developed with an end-to-end pipeline for tree diameter estimation through Semantic LiDAR Odometry and Mapping (SLOAM).

Table 2.3 summarizes the locomotion systems and sensors used by each robot mentioned in this subsection.

Table 2.3 - Comparison of the analysed data collection robots

Robot	Locomotion System	Sensors Used
Environmental Hybrid Robot (EHR) [26]	Wheel-legged	GPS, 3D camera
UAV robot 1 [27]	UAV (aerial application)	GPS, Hyperspectral camera
UAV robot 2 [28]	UAV (aerial application)	GPS, IMU, Infrared camera, RGB camera
UAV robot 3 [29]	UAV (aerial application)	LiDAR

2.2.4. Forest cleaning robots

Forest cleaning robots (Figure 2.4) are designed with the goal of clearing biomass accumulation in forests and, as such, require specific tools to achieve said purpose (e.g., mulchers, chippers, grinders). The ability to reduce flammable material in a forest can severely impact wildfire spread, so, it is only natural that increasing developments are being made in this area, howbeit the field remains underdeveloped.

(a) (b)

Figure 2.4 - Examples of robots used in forest cleaning applications: (a) Ranger from the SEMFIRE project [30], (b) AgRobV18 [31]

The SEMFIRE project [30] was developed to reduce biomass accumulation in forests. It uses a multi-robot system where a group of small UAVs, called Scouts, scan an area to locate regions of interest for the Ranger robot, an adapted Skidsteer platform, to perform the cleaning task. Making use of Global Navigation Satellite System (GNSS), LiDAR, and stereo, multispectral and infrared cameras the Ranger robot identifies, cuts and grinds vegetation, turning it into mulch.

The AgRob V18 [31] is a forest robot designed to collect organic material in forests. It utilises a modular sensor tower and thermal and RGB cameras to detect the fauna and flora around it. Due to its diesel engine, the robot's vibration affects the IMU data, which in turn impacts its ability to perform autonomous navigation. To improve the robot's performance, the team used Lightweight and Ground-Optimized LiDAR Odometry and Mapping (LeGO-LOAM).

The diesel engine problem presents itself as the main internal obstacle to overcome when developing autonomous solutions, as the use of sensors, especially those most affected by vibrations, such as LiDAR or IMU, is severely impaired by the engine's operation. Due to parameters such as unbalanced reciprocating and rotating parts, cyclic variations in gas pressure generated by the combustion process, misfire, and inertia forces of the reciprocating parts, significant levels of vibration are induced in any internal combustion engine (ICE) [32].

To reduce the engine vibration, proper mounting must be provided as dampers at the interface of the engine and chassis [33]. As other solutions usually require changing either the design of crucial engine components or altering the properties of the fuel blends [32].

Table 2.4 summarizes the locomotion systems and sensors used by the two robots mentioned in this subsection.

Table 2.4 - Comparison of the analysed forest cleaning robots

Robot	Locomotion System	Sensors Used
Ranger [30]	Tracks	GNSS, LiDAR, Stereo camera, Multispectral camera, Infrared camera
AgRob V18 [31]	Tracks	GNSS, LiDAR, Infrared camera, RGB camera, IMU

Both robots have the LiDAR sensor installed in the highest point of their structures and all cameras are also mounted in elevated positions with unobstructed fields of view.

2.3. Vibration damping techniques

Vibrations can adversely affect the tasks carried out by automated or remote operated robots, as individual components in a vehicle can create unwanted vibrations or noises that can disrupt sensors functions. Moreover, resonance can occur between individual sources, leading to more damaging global vibrations. Consequently, the field of vibration suppression is of extreme importance.

Traditional approaches to vibration damping can be divided into two categories: internal vibration mitigation and external vibration mitigation.

Internal vibrations refer to vibrations caused by the vehicle's internal components, such as the engine and the transmission. Internal vibration damping is mostly focused on limiting resonance between internal components and resonance between components and the vehicle itself [34]. External vibrations refer to vibrations caused by external effects, like navigating unstructured terrain.

Vibration damping techniques can be further divided into active and passive approaches. Passive vibration mitigation translates to a conventional fixed-suspension system installed on a vehicle, whereas active vibration suppression solutions complement the passive suspensions with controlled actuators [35].

2.3.1. Passive vibration damping approaches

Passive damping solutions can still be further divided into shock absorbers and dampers.

Mechanical shock is a high amplitude impulse that usually involves large forces and accelerations over a very short time, as such, shock absorbers work by reducing the forces

generated and normally consist of elastic elements [36]. Examples of typical commercially available shock absorbers are helical springs and rubber buffers, presented in Figure 2.5.

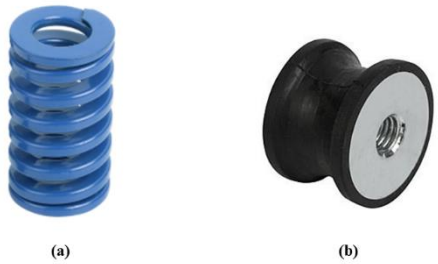

Figure 2.5 - Examples of shock absorbers: (a) Helical spring [37], (b) Rubber buffer [38]

Dampers, on the other hand, aim to reduce more standard vibrations. Vibration differs from shock in that it has a periodic nature with lower amplitude variations, so, dampers do not need to withstand high force, brief impulses, but rather low intensity, continuous solicitations. Common examples of dampers are presented in Figure 2.6, these are:

- Viscoelastic layers – also called damping plates, are layers made of materials capable of dissipating the vibrational energy through their deformation [39];
- Gimbals – a gimbal is a support system, usually seen in UAVs, that allows rotation of an object about an axis. A three-axes gimbal, for example, is enough to fixate an IMU in inertial space, thus allowing to maintain the orientation of the IMU.

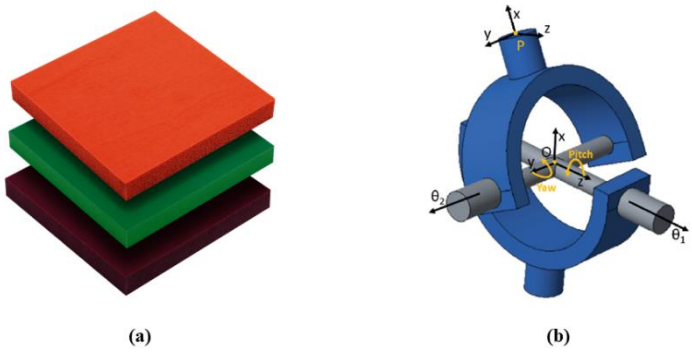

Figure 2.6 - Examples of dampers: (a) damping plates [40], (b) CAD model of a gimbal mechanism, retrieved from [41]

However, it should be noted that gimbal frames, and similar solutions, not only help reduce unwanted vibrations in the three translational axes, but also stabilise the components in the rotational space. This can be advantageous for some applications, but detrimental to others.

Finally, wire rope isolators (WRIs) are a different type of passive isolators which exhibit non-linear behaviour in both elastic stiffness and damping [42] and provide

multidirectional protection not only against shock but also against periodic vibrations, all while being less susceptible to the detrimental effects of harsh environments and keeping a low manufacturing cost [43]. Polycal WRIs offer the best performance when the isolation of lightweight sensors is concerned, notable examples are the wire rope isolators developed by Socitec [44] and by Vibrostop [45].

(a) (b)

Figure 2.7 - Examples of polycal wire rope isolators: (a) MP2 series from Socitec [44], (b) AVAU HF series from Vibrostop [45]

Polycal WRIs also have the added advantage of being easily reproducible without relying on complicated manufacturing processes, as they consist simply of steel cable strands held between two retainers. And, as they are effective in decreasing vibrations of a periodic nature, their application is highly valuable in isolating the vibrations generated by internal combustion engines.

2.3.2. Active vibration damping approaches

Gimbals can also be used as active damping solutions if the stabilisation process is accomplished through the use of motors and not in a passive way. In [46], a gyroscopic stabiliser, constructed with a gimbal frame, was used to reduce the mechanical vibrations affecting a 3D mapping device mounted on an UGV (Unmanned Ground Vehicle). The stabilisation process is accomplished by driving the gimbal motors in answer to reception of a signal from an IMU sensor. The obtained results, which can be seen in the graphs on Figure 2.8, Figure 2.9 and Figure 2.10, show the capabilities of such devices acting as vibration damping solutions. In the left of each pair are the time-based measurements of the sensor without the stabiliser while the right are the ones with the effects of the stabiliser. Note that the authors did not specify the amplitude units.

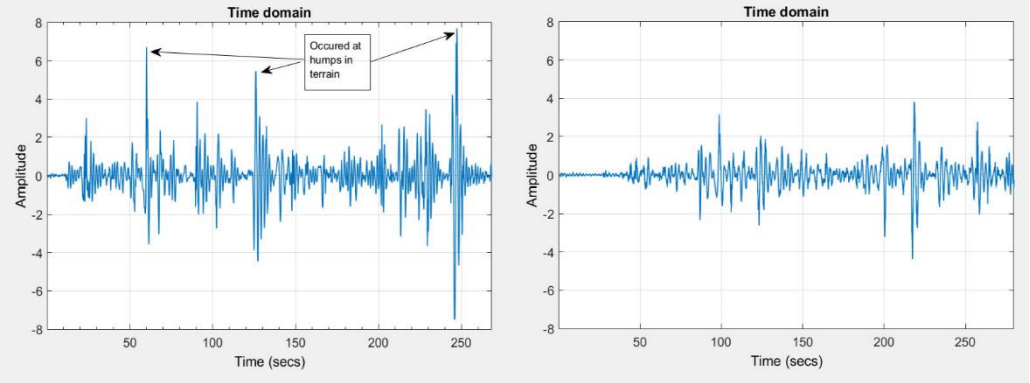

Figure 2.8 - Time-based representation of acceleration measurements from X-axis, retrieved from [46]. (Left) measurements without stabiliser, (Right) same measurements with stabiliser

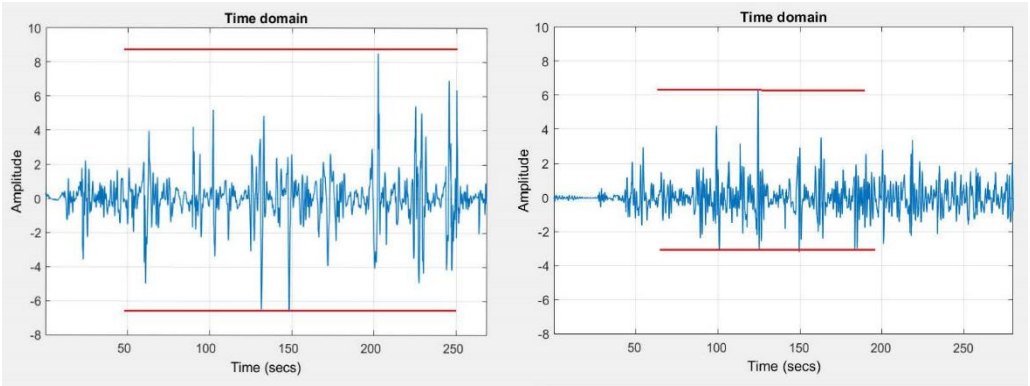

Figure 2.9 - Time-based representation of acceleration measurements from Y-axis, retrieved from [46]. (Left) measurements without stabiliser, (Right) same measurements with stabiliser

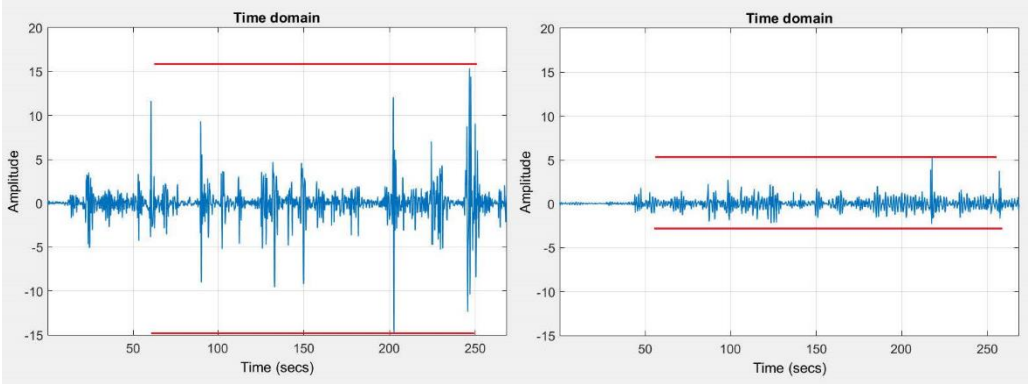

Figure 2.10 - Time-based representation of acceleration measurements from Z-axis, retrieved from [46]. (Left) measurements without stabiliser, (Right) same measurements with stabiliser

However, most methods for active vibration damping focus on terrain determination based on vibration analysis, which then determine the robot's course of action for how to best mitigate said vibrations [47], [48].

In [49] a control system was designed to modulate the velocity of a vehicle in order to minimize sudden impulses and prevent damage to passengers and cargo. The control system provides a method of navigating unknown terrain while limiting damage caused by high-

frequency vibrations without the need for prior terrain identification. Although effective, such a solution would require constantly changing the speed of the vehicle, which in many applications is not a feasible condition to meet.

Variable Stiffness (VS) and Variable Damping (VD) systems effectiveness on vibration damping has been thoroughly tested [50] and these systems superiority on reducing unwanted vibrations has led to suspensions with the ability to vary their stiffness and damping to be more and more common [51], [52].

Sun et al. [53] present a design of a magnetorheological (MR) vehicle suspension with tunable stiffness and damping characteristics, capable of reducing the sprung mass accelerations with great efficacy when compared with other suspensions. However, MR suspensions are not adequate in the presence of sensors affected by magnetic fields, as they will disrupt measurements.

2.4. Influence of dust and other particulates on sensor accuracy

Dust and other particulates, such as smoke, rain and water vapour, can severely impair a robot's capability of conducting automated tasks, specifically when said particulates prove detrimental to sensor accuracy, namely sensors that require the use of cameras or light sources.

Phillips et al. [54] studied the behaviour of different LiDAR sensors in the presence of dust and concluded that the effect of dust on LiDAR measurement is systematic and, while being clear that said effect is evident, the point cloud contains significant information relevant to the perception functions, and also, the impact of dust in the sensor's field of view is highly structured.

Their main finding was that LiDAR sensors exhibit four clearly different behaviours, as shown in Figure 2.11:

(a) where dust is sparse, they image unimpeded;
(b) in sufficiently dense dust, they image the surface of the dust cloud;
(c) there is a transition condition between (a) and (b) determined by the density of the dust and reflectivity of the target where the return pulse captures the range to the surface of the dust cloud and the target;
(d) under certain circumstances, no range measurement is returned.

Also, where dust is imaged (specifically behaviours (b) and (c)), the measured range is to the front of the dust cloud.

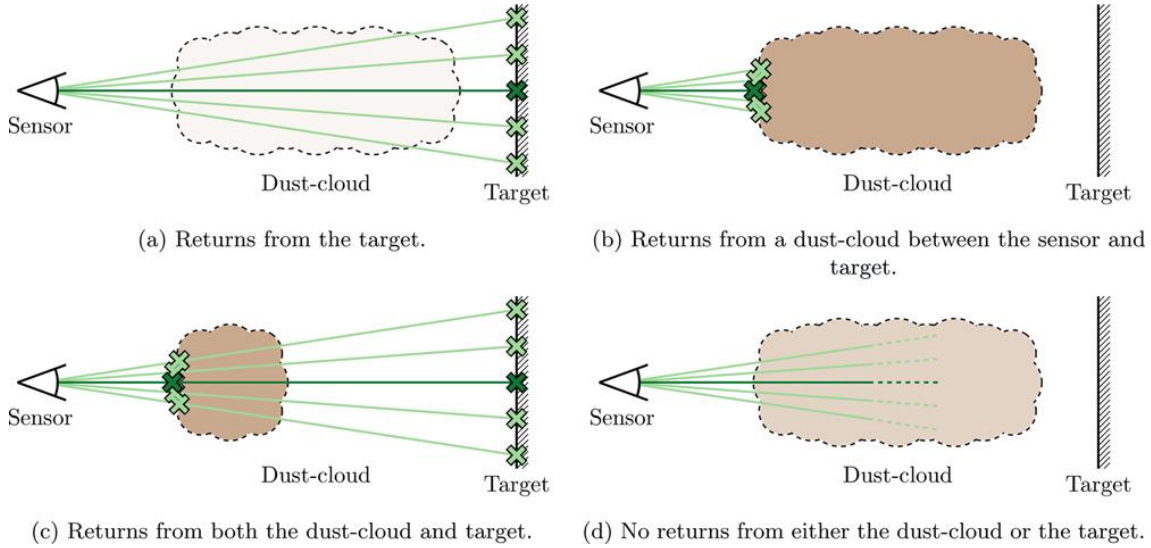

Figure 2.11 - The four measurements behaviours exhibited by LiDAR sensors when in the presence of dust, retrieved from [54]

In the presence of rain, Ryde & Hillier [55] showed that LiDAR accuracy, although generally robust in sparse rain, quickly degrades in heavy mist, where higher light refraction is expected. Additionally, rain will also limit the range of IR measurements due to the scattering of light off droplets of water [56], which present severe performance degradation in the 100-500 metre range.

Starr & Lattimer [57] performed experimental studies to quantify the performance of several robotic navigation rangefinding technologies and camera systems in fire smoke environments, testing sensor performance for dense, low temperature smoke (<1 m visibility and <100 °C) and light, high temperature smoke (>5 m visibility and >250 °C). Their primary conclusions included:

- LiDAR shows strong attenuation when visibility drops below 5 m, however, it does not appear to be affected by temperature;
- Visual cameras work poorly below a visibility of 8 m and fail with either too much or too little light present in the scene;
- Thermal IR cameras maintained accuracy in both light and dense smoke conditions.
- Sensors with longer wavelengths (typically above 7.5 μm) are unaffected by smoke.

Likewise, Pascoal et al. [58] determined LiDAR sensors perform poorly in smoky conditions, while also concluding that the presence of water vapour will either lead to erroneous measurements or saturate the sensor, producing no measurement.

Lastly, according to Pan et al. [59], IR cameras respond to the presence of dust depending on the dust location (Figure 2.12):

(a) when dust is present on the surface of the measured object, the area covered by it shows significantly lower temperature than that of the area not affected by dust;

(b) when dust is present on the lens of the camera, temperature of part of the blackbody target surface becomes lower, however, the difference is minimal when compared with the other situations;

(c) for dust in the optical path, temperature measurements show varying degrees of error.

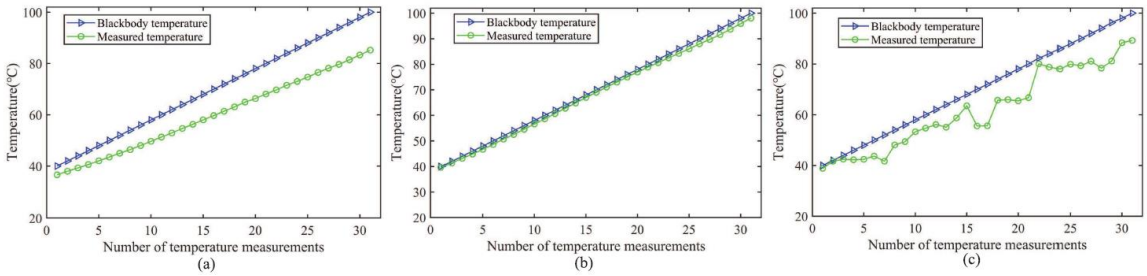

Figure 2.12 - Temperature measurement results under the dust influence. (a) Dust on the surface of measured object. (b) Dust on the camera's lens. (c) Dust in the optical path. Retrieved from [59]

2.5. Influence of time of day on sensor accuracy

Sensors can broadly be divided into two categories: passive and active sensors. While passive sensors require an external source of energy, like sunlight, to obtain measurements, active sensors use their own sources of radiation to generate signals which, when reflected from the intended target, allow for measurements to be made. In the current application, both the stereo depth camera and the multispectral camera are classified as passive sensors, the LiDAR and IR sensors fall under the active sensors category, and the Duro Inertial (GPS + IMU combination) is obviously not affected by lighting conditions but does not fall under either category.

Given this distinction, passive sensors are expected to respond in different ways to the changes in lighting that occur throughout the day and especially poorly to either the absence

of light sources or the exposure to overwhelming light sources. Contrastingly, active sensors should not have much difficulty working in differently lit environments.

2.5.1. Sunlight influence

LiDAR sensors work mostly well under direct sunlight, whereas most cameras, namely visible RGB cameras, have the problem of image saturation due to sun glare [60].

Outdoor temperature measurements in the infrared range can be very inaccurate because of the influence of solar radiation reflected from a measured object, leading to the measured temperature being higher than the real one [61]. This measurement error increases for low-emissivity and low-temperature objects [62].

2.5.2. Nighttime influence

Pinchon et al. [63] conducted experiments on four different spectral bands, including visible RGB and Long-Wave Infrared (LWIR), the spectral band of the IR camera used in this work. They concluded that the LWIR camera allowed effective pedestrian and animal detection in full darkness, while the visible RGB camera was ineffective in such conditions. LiDAR, on the other hand, is unaffected by the lack of light sources.

2.6. Conclusions

Apart from the sensor-specific constraints, detailed in section 1.3.2, the effect of more general constraints was studied in sections 2.3 through 2.5.

One of the most important conclusions to draw from the work to be developed is how each sensor's strengths can be used to diminish the impact of the remaining sensors' weaknesses to ensure that the complete sensory system performance is guaranteed in any environment, regardless of conditions. The goal is to add redundancy to the system, so that performance can be assured with a sufficient safety margin.

Table 2.5 summarises the effect of different constraints on each of the sensors used in the current application.

Table 2.5 - Effect of different constraints on the sensors to be used; −, +, ++, +++ translate to unaffected, slightly affected, affected, and severely affected, respectively

Sensor name	Type of sensor	Vibrations	Dust or smoke	Rain	Sunlight	Darkness
Puck™	LiDAR	++	++	+	−	−
Intel® RealSense™ D435i	Stereo depth camera	+	++	+	+++	+++
Duro Inertial	GPS + RTK + IMU	+++	−	−	−	−
FLIR ADK	IR camera	+	+	+	++	−
Genie Nano-CL C2420	Multispectral camera	+	++	+	+++	+++

3. SENSOR FIELD TESTING

The tests conducted to assess the performance of the machine itself and of each sensor are presented in this chapter.

A first, broader field test, conducted before addressing the specific constraints, made it possible to observe the problems that standard machine operation was faced with.

As each constraint affects the sensors in unique ways, after the initial field test they were studied as separate problems, and individual solutions were proposed to mitigate the impact of each one. The work developed for each constraint is presented, outlining the methodology followed as necessary. The procedures followed are described in detail and, in tasks where measurements were taken, the instruments used are introduced.

Figure 3.1 shows a detailed 3D model of the robotic platform, with the main components numbered and identified.

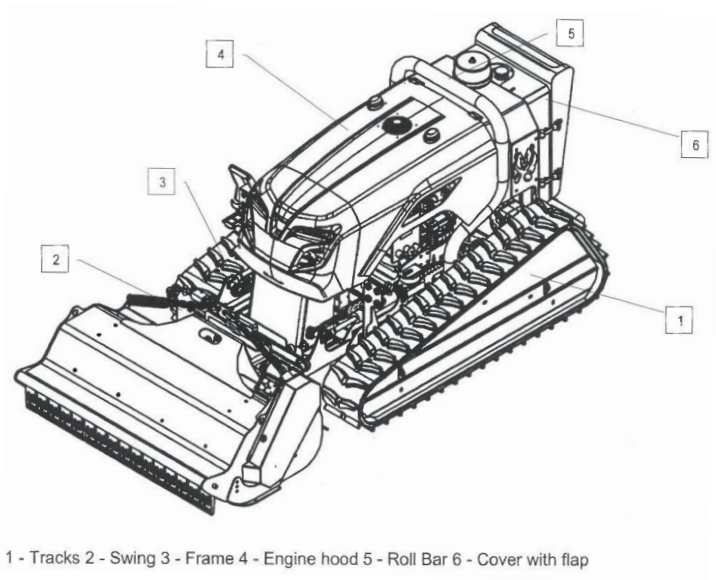

Figure 3.1 - 3D model of the robotic platform developed by MDB Technologies, retrieved from the "Operations and Maintenance Manual"

A 3D, simplified CAD (Computer Aided Design) model of the robotic platform was created with the purpose of aiding the display of specific components (see Figure 3.2). This simplified model contains additional parts, specifically the available sensors and their respective supports, these new parts were also physically added to the robotic platform so sensor performance could be tested.

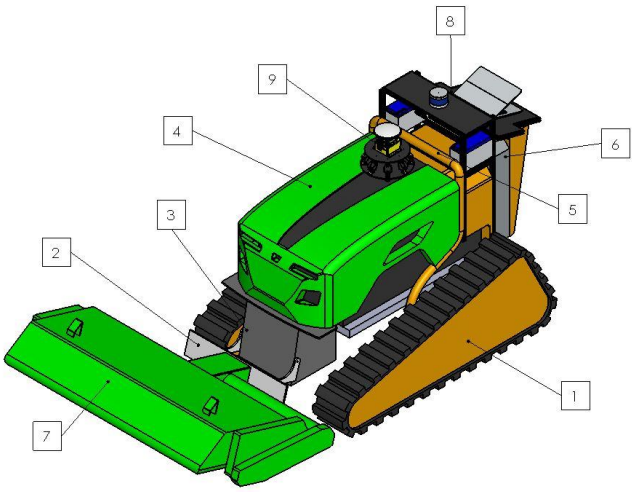

1- Tracks; 2 - Swing; 3 - Frame; 4 - Engine hood; 5 - Roll bar; 6 - Cover; 7 - Mulcher tool; 8 - Support for sensors, batteries and control unit; 9 - Duro Inertial

Figure 3.2 - 3D simplified model of the robotic platform developed for purposes of illustration throughout this thesis

Some limitations made certain parts of the proposed work impossible to complete, namely:

- Lack of access to two of the specified sensors, IR and Multispectral cameras, due to unforeseen shipping delays, led to the impossibility of conducting experiments with these cameras. As such, guidelines for these two sensors were derived from the researched state-of-the-art;
- Due to the beginning of the fire season in Portugal, the use of the mulcher tool was forbidden after a specified date, which made further data collection tied to the mulcher operation impossible;
- As the machine is not yet capable of operating in the presence of rain, due to the installed components not having been assembled to withstand contact with water, guidelines for operating in rainy conditions were derived exclusively from the researched state-of-the-art;
- Due to working restrictions, the machine was not tested during nighttime. Note that development of the system is not aimed at nighttime operations, regardless, the possibility of operating without natural light sources is discussed in the “Sunlight/Darkness” subchapter;
- Lack of access to the machine towards the end of the thesis, due to unforeseen mechanical issues, limited the number of tests that could be carried out.

3.1. First field test

A first field test was conducted with the goal of identifying the main problems with the application. The machine was initially operated in a road paved with asphalt, before being taken to an area with mixed vegetation, consisting of bushes, grasses, and trees, where the mulcher tool could be employed.

On this first test the machine was equipped with the Duro Inertial (GNSS + RTK system), the Puck™ (LiDAR camera), and the Intel® RealSense™ D435i (Depth + RGB camera), as well as batteries for powering the Duro Inertial and a laptop to act as a control unit. Figure 3.3 lays out the positioning of these components. A ground station was also used, as it was needed to complete the RTK system.

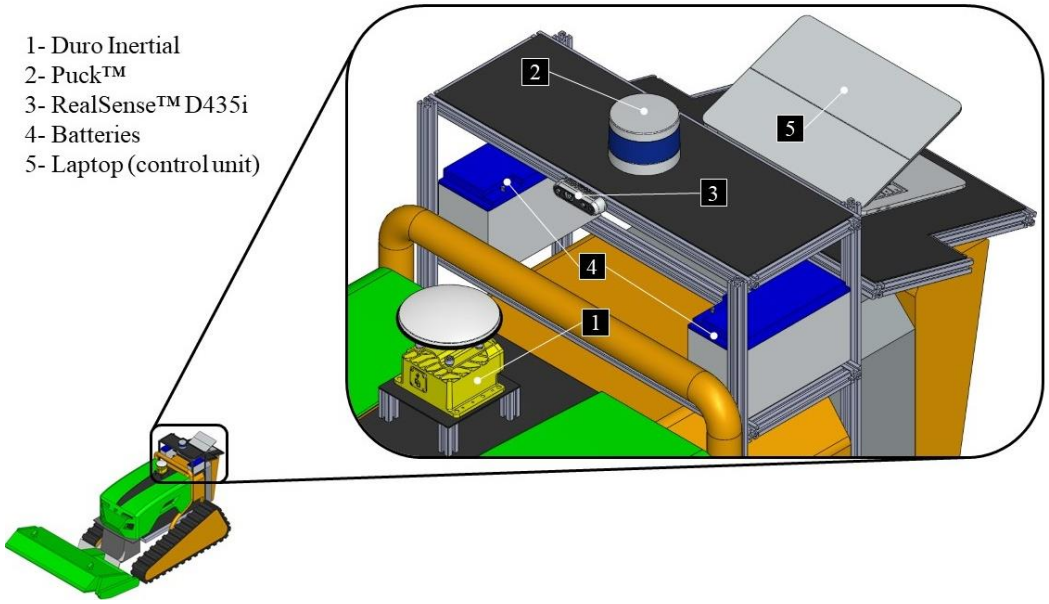

Figure 3.3 – CAD model of the components installed for the first field test

The main conclusions taken from this first field test were:

- The machine, when accelerating from a fully stopped position or fully stopping while in motion, will most times do so in an abrupt manner. This transmits a considerable shock through all the components, which, in our test, led to the dislodgement of some sensors and the disconnection of several cables;
- The so-called “jello effect”, a phenomenon that appears when a camera is vibrating at a high frequency, usually seen in drones [64], was noticeable in the videos recorded by the Intel® RealSense™ D435i camera. This phenomenon was present anytime the engine was turned on, even when the machine was stopped;

- GNSS connection through the Duro Inertial was slow, despite assuring an open sky condition. Additionally, when under the canopy of trees, the signal became inconstant and unreliable;
- RTK connection between the ground station and the Duro Inertial was stable when a direct line of sight between the two components was established, but quickly failed when said direct line of sight was obstructed;
- The Duro Inertial shook a lot, mainly due to the internal vibrations created by the combustion engine's working process. This has severe repercussions on IMU measurements;
- LiDAR measurements were corrupted, which made it impossible to conclude anything of the Puck's operating capabilities;
- The vehicle's range of operation, motor speed wise, was observed as being between 900 and 2100 rpm (revolutions per minute) through most of the test, with the noted exceptions not warranting a focused study. This is the range that is used to limit the analysis in the "Vibrations" subchapter.

3.2. Temperature

3.2.1. Methodology

To determine if temperature plays a factor in sensor performance, measurements were taken during a one hour long test where the machine was operated outside, in a day with minimal clouds and an ambient temperature averaging 20 °C, in an area with mixed vegetation that allowed intermittent use of the mulcher tool, mimicking standard operation.

A T1020, a thermal imaging camera produced by Teledyne FLIR [65] with a thermal sensitivity of under 20 mK, was employed to measure the temperature changes in the machine during the field test. Temperature values were registered at the half an hour and one hour marks to understand the temperature changes in the machine.

Table 3.1 shows the working temperatures range of each sensor, as well as of the proposed control unit.

Table 3.1 - Temperature range where working conditions are assured for the control unit and each sensor

Control unit/ Sensor name	Jetson Xavier NX	Puck	Intel RealSense	Duro Inertial	FLIR ADK	Genie Nano
Working temperature [°C]	0 to +90	-10 to +60	0 to +35	-40 to +75	-40 to +75	-20 to +60

3.2.2. Results

Figure 3.4 and Figure 3.5 were created with the Teledyne FLIR software "Thermal Studio Suite" through image analysis and show the machine's temperature after half an hour and a full hour of operation during the first field test, respectively.

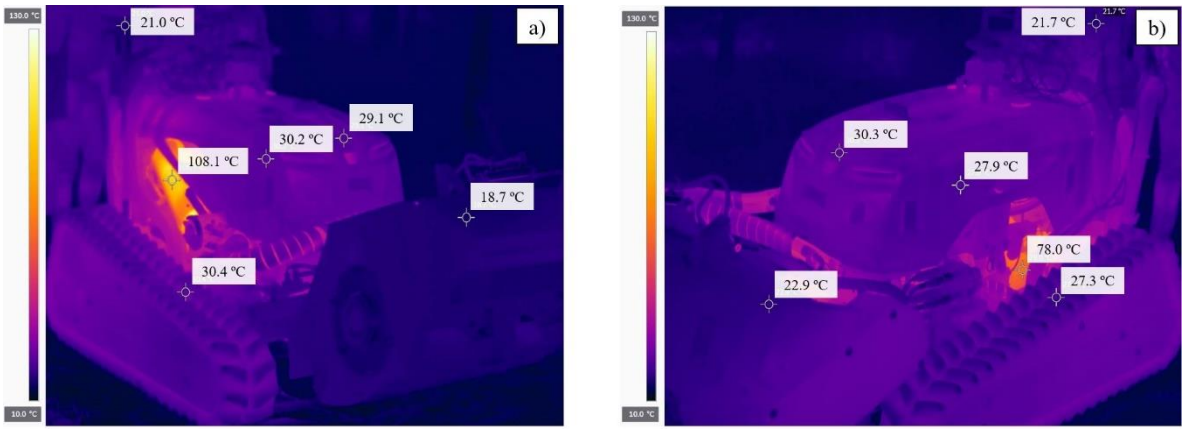

Figure 3.4 - Machine's temperature after half an hour of operation

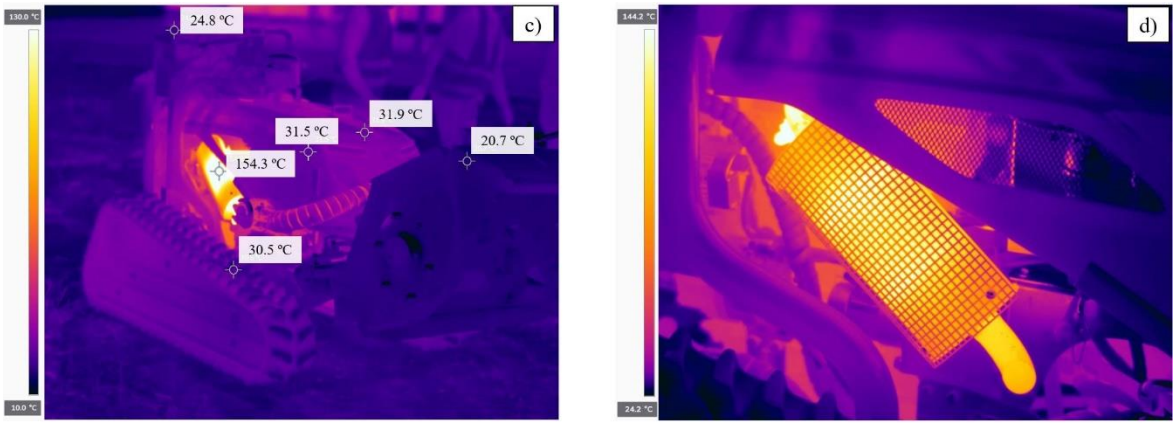

Figure 3.5 - Machine's temperature after a full hour of operation

A direct comparison can be established between images a) and c) through the temperature spots highlighted in order to understand where the temperature increase is more noticeable. It can be observed that the outside bodies of the machine, namely the hood, tracks, mulcher and the top support, do not have a noteworthy temperature increase; only the

interior zone of the vehicle, specifically the engine and the exhaust, have a notable increase, this can be further confirmed by observing image d).

The only concerning aspect derived from the machine's temperature increase is the maximum operating temperature of the Intel® RealSense™ D435i camera, which is limited at 35 °C. It is important to note that the manufacturer does not claim that the camera will stop working when the temperature increases past this point, only that performance will decrease (i.e., sensor damage is not in question).

Figure 3.6 shows the temperature of both the D435i camera and the Puck sensor after the conclusion of the first field test. The photo was taken in the shade to avoid influencing the measurements due to reflected solar radiation.

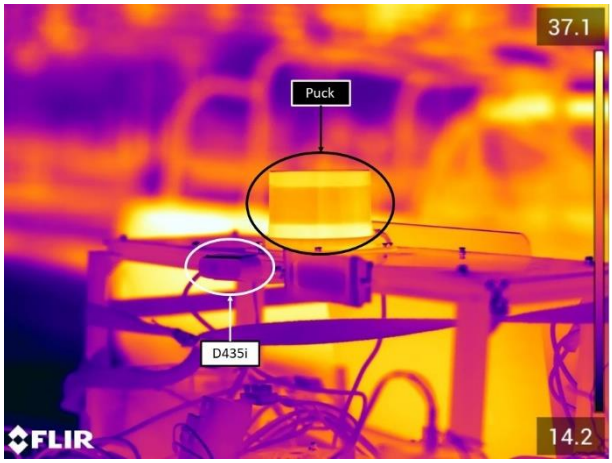

Figure 3.6 - Temperatures of the stereo depth camera (D435i) and the LiDAR (Puck) after the field test

During this test, the stereo depth camera did not surpass the 35 °C limit. However, as this is a fairly low temperature limit, it cannot be assured that in hotter days, or if the camera is exposed to the sun for longer periods of time, its temperature will not exceed the limit. Thus, it is recommended to cover the camera to avoid direct exposure to sunlight, leaving space for the cooling of the camera (above and below) and the lenses unobstructed. Alternatively, other camera options should be considered if the camera proves unreliable.

The LiDAR sensor is shown to heat up more than its surroundings, with most of the heat being a product of the Puck's own functioning. Still, its maximum operating temperature of 60 °C is far from being reached.

Lastly, when the IR camera becomes available, tests should be conducted to assess if the heat from the combustion engine and the exhaust pipe is enough to skew the results of thermal imaging or if no impact is seen.

3.3. Dust and other particulates

The accumulation of dust and other debris will negatively impact the sensors' ability to perform as intended. Although not much can be done to reduce the presence of dust and other particulates in the air (barring reducing the use of the mulcher, which contradicts the purpose of the machine), dust accumulation on the machine can be measured and accounted for, which in turn allows for solutions to alleviate this problem to be proposed.

3.3.1. Methodology

To measure dust and debris accumulation, glass panels were mounted on several locations throughout the machine to evaluate the dust accumulation in different places. All panels were identical, composed of the same glass, with a dimension of 40x100 mm and a thickness of 2 mm. Figure 3.7 shows the casing used to frame each panel, where on the left a slit is present to insert the glass panel into the casing.

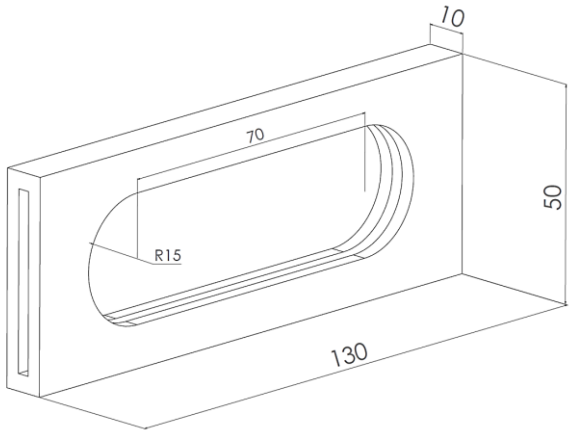

Figure 3.7 - Casing used to frame each glass panel, with dimensions, in mm

Figure 3.8 shows the location of the nine glass panels mounted onto the machine and used to quantify the accumulation of dust and other particulates.

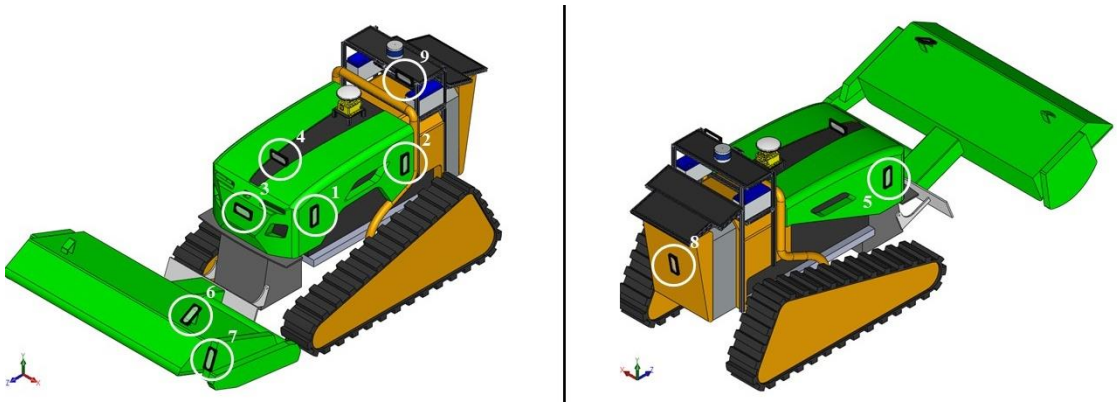

Figure 3.8 - Positioning of the glass panels mounted throughout the machine

Tests were carried out with and without the use of the mulcher, so that conclusions could be drawn for both cases.

Photos of the glass panels were taken with the use of a box and a LED light, so that the only light source passing through the panels was illuminating all the debris attached to each glass panel. Figure 3.9 shows the assembly used.

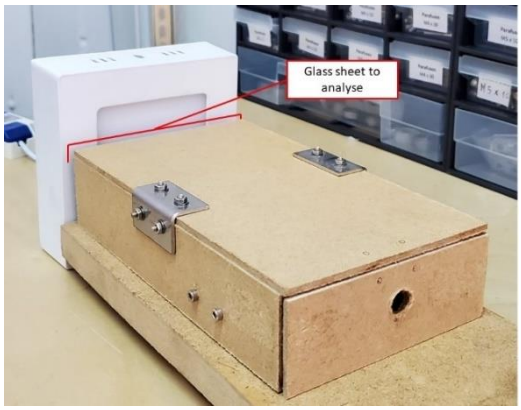

Figure 3.9 - Box used to photograph the accumulation of dust in each glass panel

Figure 3.10 shows a comparison between an example of a cleaned glass panel and a glass panel with accumulated debris.

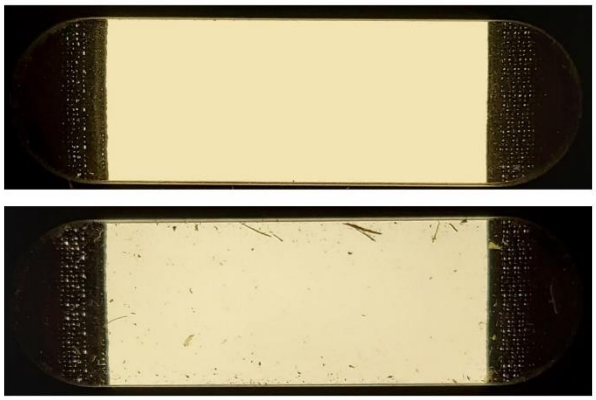

Figure 3.10 - Comparison of a clean glass panel (Top) and a glass panel with accumulated debris (Bottom)

The images were then greyscaled and, afterwards, each pixel was transformed into either a white or a black one (making the image exclusively black and white), this process was done with the use of the MATLAB software, developed by MathWorks.

This was done to make the number of white pixels in each image quantifiable, which allows a direct correlation between the percentage of white pixels in an image and the dust accumulation in a specific glass panel to be established. Figure 3.11 illustrates the described process.

Figure 3.11 - Image analysis process, from coloured to exclusively black and white

3.3.2. Results

To study the dust accumulation when the mulcher is not in use, several outings were completed with the machine in different environments, including paved roads, dirt-based terrains, and forest environments. The glass panels were never cleaned, replaced or removed between outings, so the results show a cumulative examination of the dust accumulation.

Table 3.2 shows the percentages of white pixels present in each glass panel. It can be observed that only one panel accumulated significant debris, that being the number 8 panel, i.e., the panel mounted on the rear of the vehicle, directly on the back grille, through where the back fan expels debris.

Table 3.2 - Percentage of white pixels for each glass panel without the use of the mulcher tool

Glass Panel nº	1	2	3	4	5	6	7	8	9
% of white pixels	99.1	99.2	99.4	99.2	99.3	99.4	99.8	97.5	99.8

Thus, it can be concluded that when the mulcher is not in use, no significant dust build-up takes place, except on the back grille, which as such should be discarded as a place for sensors mounting.

In order to quantify the dust accumulation when the mulcher is used, the machine was employed to thin different types of vegetation in a forest environment.

When the mulcher is in use, results show that dust accumulation is more prevalent directly on the mulcher tool, i.e., panel number 6 (an expected result, as concentrations of debris are higher closest to where vegetation is being thinned).

Apart from the glass panel mounted on the tool, the panels installed on the hood of the vehicle (numbers 1 and 2 on the left side, 5 on the right, and 3 and 4 on the top of the hood) show considerable dust accumulation. Overall, the only location where minimal dust build-up takes place appears to be on the top support (glass panel number 9), created for the first field tested and used to test sensor performance. Table 3.3 shows the percentages of white pixels present in each glass panel.

Table 3.3 - Percentage of white pixels for each glass panel with the use of the mulcher tool

Glass Panel nº	1	2	3	4	5	6	7	8	9
% of white pixels	98.5	97.4	98	97.9	97.6	95.7	98.1	98	99.8

3.4. Vibrations

From the first field test carried out, it became clear that the internal vibrations, generated by the combustion engine working process, were more detrimental to sensor performance than the external vibrations caused by navigating through unstructured terrain, so, vibration damping solutions were directed at reducing internal vibrations.

The shock sustained by the machine when accelerating from a fully stopped position or fully stopping while in motion, was also of concern, as it led to the dislodgement of some sensors. But the solution to this problem should be to introduce a gradient of acceleration/deceleration for non-emergency situations, to reduce the occurrence of sudden changes in velocity.

3.4.1. Methodology

Vibrations were evaluated with the Hex Cube Black flight controller [66] (previously known as Pixhawk 2.1) which comes equipped with a MPU9050 IMU, the sensor used to measure the vibrations. The vibrations were quantified through the amplitude of the accelerations measured in the three axes (x, y and z), so only the accelerometer function of the IMU was used. The accelerometer function had a predefined sample rate of 25 Hz, which was the one used for all analyses.

The sensor was always mounted with the same orientation in order to assure coherent measurements in the three axes.

Tests were conducted with reference to the engine's rotation speed, continuously increasing it according to the values observed in the first field test, i.e., always keeping the rpms inside the range of 900 to 2100 rpm. Due to the inability to yet control the engine speed, the native remote control had to be used, which in turn did not allow full control of the engine's speed, as it uses a simple 3 position joystick (rest, up, down) which was incapable of assuring constant intervals when increasing rpm (see Figure 3.12).

Figure 3.12 - Native remote control for the LV400 Pro

Due to this, it was impossible to exactly match the engine speed, unless by chance, between different tests. As such, direct comparisons between two coincident spots in separate graphs, although valid, do not translate to exactly the same engine mode in both instances.

3.4.2. Tests for different locations on the machine

Firstly, tests were carried out to understand if different locations of the machine were subjected to the same degree of vibrations, or if some locations were more affected than others. The four locations tested, shown in Figure 3.13, were: on the top support where the sensors were initially mounted, on top of the centre of the hood, under the frame of the machine, and on the mulcher tool.

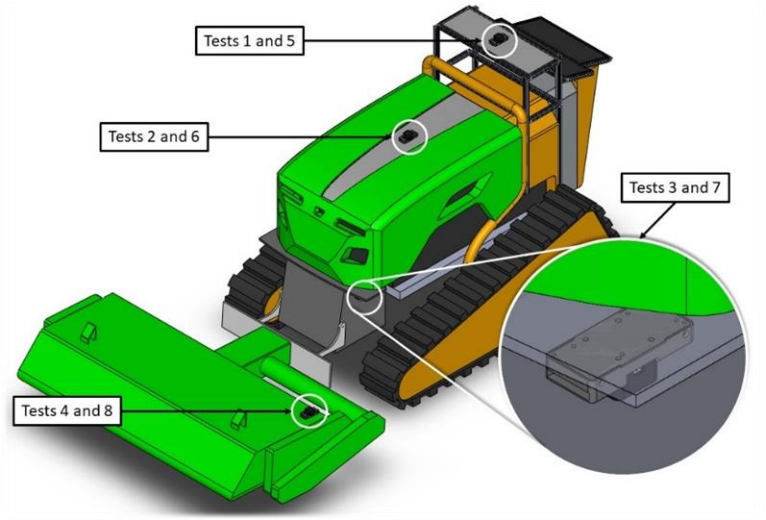

Figure 3.13 - Locations of IMU sensor for the tests conducted

It should be noted that, in the position of under the frame, the sensor was placed upside down. This changed the values of the acceleration measurements in the y and z axes to exactly their inverse, which still allows for consistent comparisons between other positions.

In total, 8 tests were conducted, one for each designated location with the mulcher being turned off and one for each location with the mulcher turned on.

Table 3.4 - Identification of the location and use of the mulcher for the tests conducted

Test nº	Location	Mulcher
1	Top Support	Off
2	Hood	Off
3	Frame	Off
4	Mulcher tool	Off
5	Top Support	On
6	Hood	On
7	Frame	On
8	Mulcher tool	On

Figure 3.14 shows the results for the first test conducted (on the top support, with the mulcher turned off). Similar results, in terms of distributions not magnitudes, were obtained for the remaining tests and are presented in Appendix B.

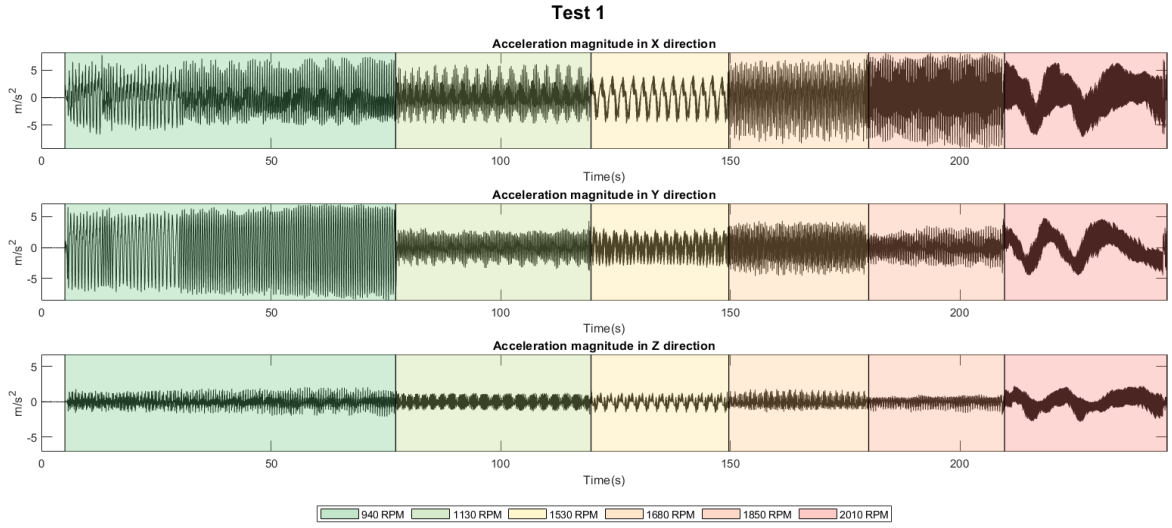

Figure 3.14 - Measured accelerations magnitudes for all 3 axes in Test nº1

It was concluded that, despite the precise magnitude not being predictable, notable differences exist between each engine mode (i.e., specific rpm value), which entails that

specific engine speeds result in specific vibrating frequencies, that can potentially be determined. This will be further analysed in section 3.4.2.1.

Table 3.5 shows the comparison of the average acceleration magnitude for all three axes between tests 2 and 1, tests 3 and 1, and tests 4 and 1, for when the mulcher is turned off. Whereas Table 3.6 shows the same comparisons but for when the mulcher is turned on, that is, between tests 6 and 5, tests 7 and 5, and tests 8 and 5.

The tables should be interpreted according to the following example:

- *For **Tests nº 2/1** the **X axis** shows a value of **0.19**, this means that for test nº 2 the average magnitude of vibrations on the x axis is 0.19 times that of test nº 1;*
- *For **Tests nº 3/1** the **Z axis** shows a value of **1.35**, this means that for test nº 3 the average magnitude of vibrations on the z axis is 1.35 times that of test nº 1.*

For the absolute average acceleration magnitude value of each test refer to Appendix C.

Table 3.5 - Average acceleration magnitude comparison between tests nº 2, 3, and 4 and test nº 1, for all 3 axes

Tests nº	X axis	Y axis	Z axis
2 / 1	0.19	0.70	2.53
3 / 1	0.23	0.25	1.35
4 / 1	0.27	0.08	0.16

For the four tests carried out with the mulcher shut off, the magnitudes of vibrations are smaller in the x and y axes on the hood and under the frame when compared to the top support but are larger in the z axis. On the mulcher tool vibrations are smaller for all axes when compared to the top support.

Table 3.6 - Average acceleration magnitude comparison between tests nº 6, 7, and 8 and test nº 5, for all 3 axes

Tests nº	X axis	Y axis	Z axis
6 / 5	0.27	0.74	2.99
7 / 5	0.41	0.22	1.43
8 / 5	0.36	0.10	0.66

When the mulcher is on, the same differences in vibrations as with the mulcher shut off are present. The mulcher tool appears to be the best location when the least vibrations

are the only goal, however, other constraints apply (such as dust accumulation which was already discussed) that will render the mounting of sensors directly on the mulcher tool invalid.

The top support also appears to be the least favourable location on which to mount sensing equipment, in terms of vibration magnitude. Nonetheless, the same reasoning as for the mulcher tool applies, when other constraints are considered, this location presents itself as more advantageous.

Table 3.7 shows the comparison, for the same location, of the average acceleration magnitude for all three axes, between the mulcher being turned on or off. That is, between tests 5 and 1, tests 6 and 2, tests 7 and 3, and tests 8 and 4.

Table 3.7 - Average acceleration magnitude comparison for each location with and without the mulcher being turned on, for all 3 axes

Tests nº	X axis	Y axis	Z axis
5 / 1	1.02	1.54	1.04
6 / 2	1.51	1.62	1.23
7 / 3	1.82	1.37	1.10
8 / 4	1.38	2.02	4.17

For all four tests locations, vibration magnitude always increases when the mulcher is turned on. This increase is much more prominent on the mulcher tool, where on the z axis the magnitude of vibrations is over 4 times larger when the mulcher is employed. In contrast, the top support is where the least increase exists, with the x and z axes increase in magnitude being almost non-existent.

3.4.2.1. Frequency analysis

As in all tests carried out a clear difference between the vibrations originated by each engine speed was observed, it was hypothesised that the specific frequencies each rpm creates could be calculated, and then countered.

Frequency analysis is the approach through which the vibration data registered in the time domain can be converted to a frequency domain, this then allows the main frequencies of the measured wave to be identified. Within the scope of frequency analysis, Fast Fourier Transform (FFT) is one of the fastest algorithms through which a discrete Fourier transform can be computed to transform data from a function of time to a function of frequency.

FFT, however, has a limit on which frequencies can be analysed for a specific data set. The Nyquist-Shannon sampling theorem [67] states that the highest signal frequency that can be adequately presented in a wave is half of the sampling rate so, because the sampling frequency used was 25 Hz, the highest frequency that can be analysed is 12.5 Hz.

Through simple observation, the vibrations generated by the combustion engine's working process are clearly above the limit of 12.5 Hz, so, although a sampling rate of 25 Hz is enough to compare the vibration magnitude between experimental tests, it is not enough to perform a complete and correct FFT analysis.

3.4.2.1.1. FFT analysis example

As an example, the measured accelerations for test nº1, specifically the accelerations registered for the 1530 rpm in the x axis, were used to perform a FFT analysis. This example serves only to show how the process of FFT analysis can be carried out, as the sampling rate of 25 Hz does not allow for a full deduction of the frequencies that actually compose the vibrations in this case.

The MATLAB software was used for this process.

After isolating the accelerations registered in the 1530 rpm range, the necessary parameters must be specified, namely the sampling frequency and the length of the data, in this case, 25 Hz and 740, respectively.

For FFT analysis, the data sample length must match a power of two (such as 256, 512, 1024, and so on), for this example the power of two above 740, 1024, must be taken as the data length.

The MATLAB software allows the implementation of an FFT algorithm [68], which implements the Fourier transform defined as follows:

$$Y(k) = \sum_{j=1}^{n} X(j) W_n{}^{(j-1)(k-1)} \tag{1}$$

Where n is the data length matching a power of two, $X(j)$ is the acceleration measured at each step, and W_n is a complex nth root of unity defined as:

$$W_n = e^{\frac{-2\pi i}{n}} \tag{2}$$

The absolute values of the Fourier transform Y can then be plotted in a frequency domain of half the sampling rate, as seen in Figure 3.15.

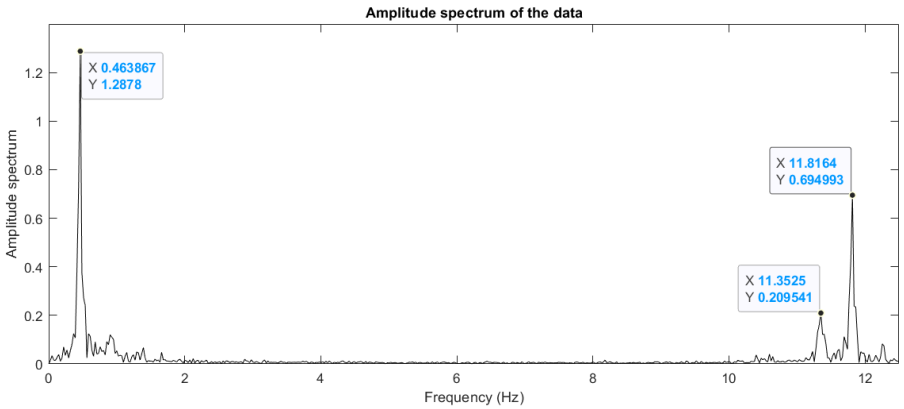

Figure 3.15 - Amplitude spectrum of the example data

In the frequency domain, the measured data has peaks at 0.46 Hz, 11.35 Hz and 11.82 Hz, with their respective amplitude. From this, a cosine function can be plotted as follows:

$$F(t) = 1.2878 \cdot \cos(2\pi \cdot 0.46 \cdot t) + 0.2095 \cdot \cos(2\pi \cdot 11.35 \cdot t) + 0.695 \cdot \cos(2\pi \cdot 0.46 \cdot t) \quad (3)$$

As can be seen on Figure 3.16 the calculated cosine function closely matches the real accelerations measured in test nº1, thus it can be concluded that the main frequencies that compose the acceleration measured in the 1530 rpm range were successfully estimated.

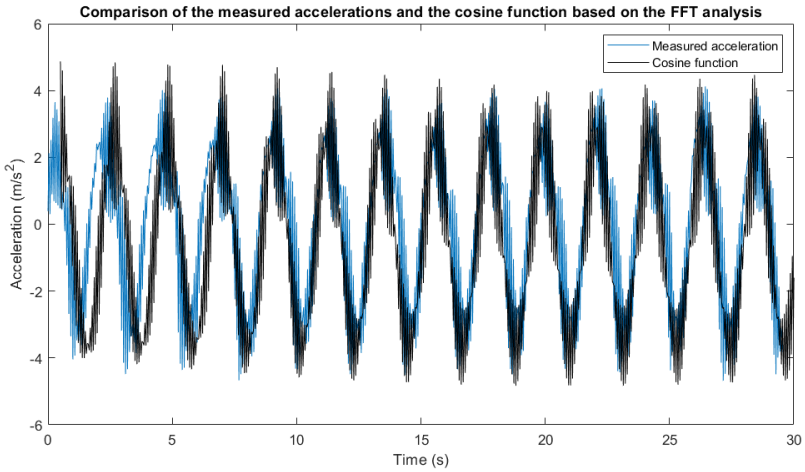

Figure 3.16 - Comparison of the measured accelerations and the cosine function based on the FFT analysis

However, these frequencies cannot be considered as correct, as the sampling frequency is not high enough. If a higher sampling frequency is achieved, by using a different sensor to measure the vibrations, and the correct frequencies that compose each engine rpm are successfully determined, then an active control system for a semi-active vibration damping solution can be envisioned.

In theory, a tuned mass damper (TMD) can be manufactured and calibrated to dampen a specific frequency [69], if a control system that measures the frequencies to which a

structure is subjected can control a TMD and direct it to dampen the main frequency that in a specific moment impacts the structure then an active tuned mass damper is created. Such examples have already been developed in [70], [71], and in others.

3.4.3. Tests for different solutions for vibration damping

In this section, the different solutions trialled for vibration damping are presented. Since for the current application we want to dampen the vibrations in the three translational axes (x, y, z) without changing the orientation of the isolated parts, i.e., without affecting the rotational axes, gimbals, or other solutions that would stabilise the components in the rotational space, were not considered as possible alternatives.

For a first approach, washers with 1 cm of thickness (see Figure 3.17), made of different materials, were used to analyse if a specific material had better vibration damping capabilities. Four materials were tested: a rubber with a hardness of Shore 90A, silicone, a foam with a density of approximately 0.042 g/cm^3 (designated “Dense Foam”), and a foam with a density of approximately 0.014 g/cm^3 (designated “Light Foam”).

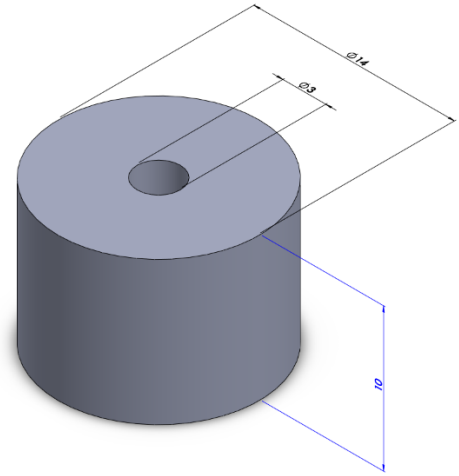

Figure 3.17 - Dimensions of washers made with different materials, in mm

These washers were used as an interface between the top support, where the sensor was mounted, and the sensor itself. The results of these analyses were compared with a hard mounted approach and also with an assembly comprised of wire rope isolators (WRIs). These wire rope isolators were made with the polycal wire rope isolators from Socitec [44] as reference, using steel cable with a diameter of 1.5 mm and terminal blocks, as shown in Figure 3.18. This approach, however crude, proved to be highly effective, as will be detailed below.

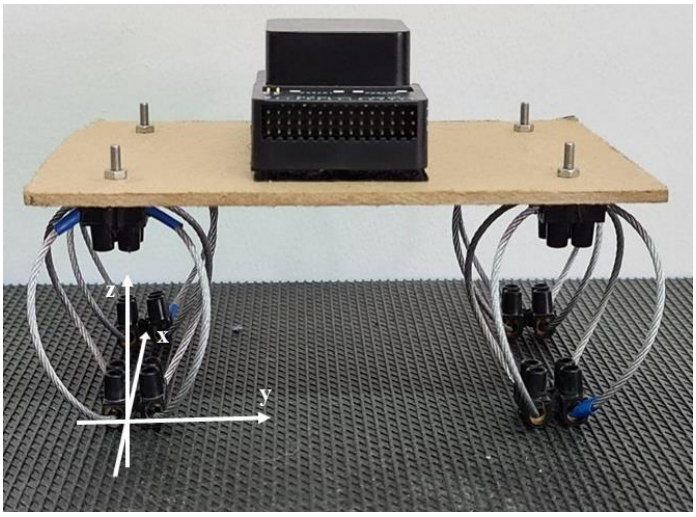

Figure 3.18 - Vibration damping solution comprised of wire rope isolators

Note that wire rope isolators have a best window of operation in terms of loading, where for a specific mass to isolate from vibrations their performance is better than for other masses. This varies with the diameter of the steel cable used, its length, the number of WRIs employed, and their disposition.

Table 3.8 shows the comparison of the average acceleration magnitude for all three axes between each solution trialled and the hard mounted alternative.

Table 3.8 - Average acceleration magnitude comparison between each test and Hard Mounted (HM), for all 3 axes

Tests	X axis	Y axis	Z axis
Rubber / HM	0.98	0.90	1.00
Silicone / HM	1.19	0.79	1.11
Dense Foam / HM	1.20	0.89	1.18
Light Foam / HM	1.20	0.93	1.41
WRIs / HM	0.03	0.04	0.79

As can be observed, regardless of their material, all washers showed minimal benefits. In actuality, other than the washers made of rubber (which equalled the performance of the hard mounted alternative), all washers had higher vibration magnitudes than the hard mounted alternative in the x and z axes.

In stark contrast, the wire rope isolators show an average acceleration magnitude that is 0.03 times that of the hard mounted solution in the x axis and 0.04 times that of the hard

mounted solution in the y axis; but show less benefits in the z axis, reducing the vibrations to just under 80% of the average values measured in the hard mounted alternative.

Figure 3.19 and Figure 3.20 show the measured accelerations in all three axes for the hard mounted and the wire rope isolators alternatives, respectively.

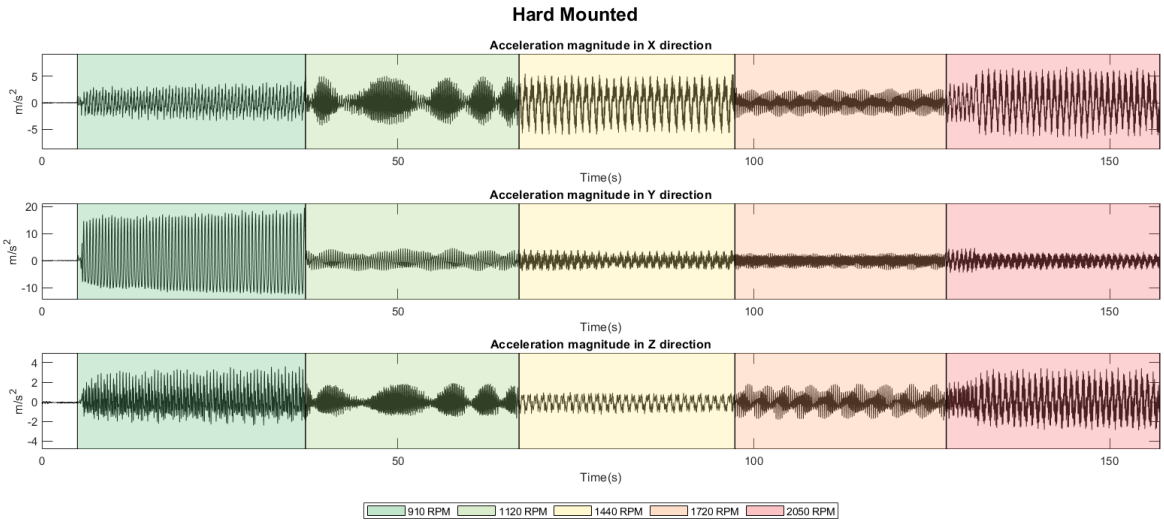

Figure 3.19 - Measured accelerations magnitudes for all 3 axes in the hard mounted alternative

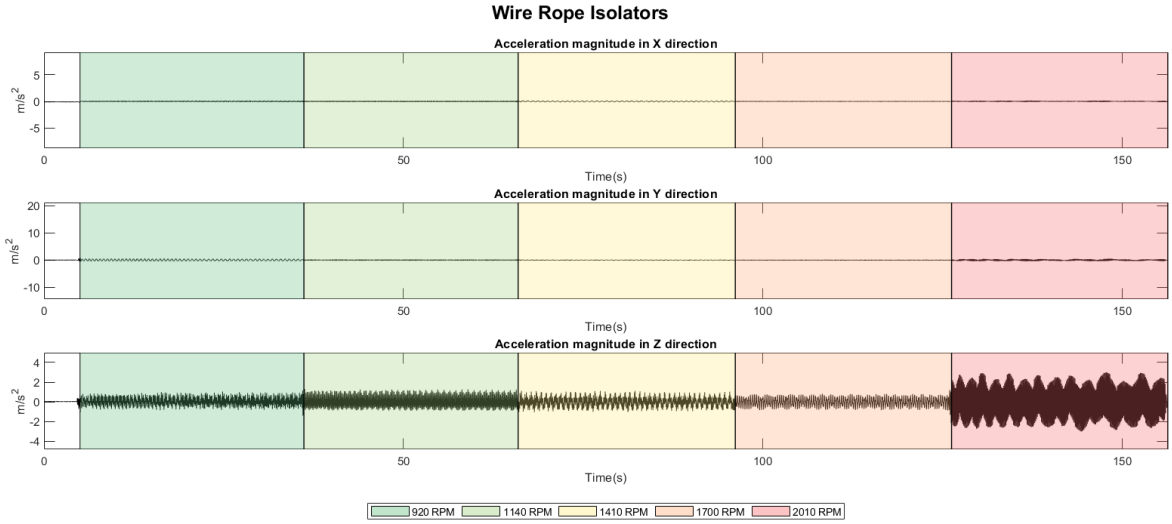

Figure 3.20 - Measured accelerations magnitudes for all 3 axes in the wire rope isolators (WRIs) alternative

As all WRIs were placed in the same position (vertically), it was hypothesized that, due to the observed results, they were especially effective in the two axes that were not their vertical axis (in this case, the z axis). As such, a combination of wire rope isolators in both vertical and horizontal positions or, alternatively, mounting the WRIs in a 45° angle, could prove more effective in damping vibrations in the three axes.

3.4.3.1. Flexible filament for 3D printing

Flexible filament was also tested as a solution for vibration damping, through 3D printing it was theorised that different designs could be 3D printed with flexible filament, thus allowing complex geometries to be employed as vibration damping solutions. However, the available filament (Nature3D's Elastic Filament [72]) had a hardness of Shore 95A, which proved too rigid and had minimal elastic return in order to constitute a sensible solution.

3.4.4. The use of wire rope isolators

Given their proven effectiveness, wire rope isolators were henceforth considered as the best possible solution for vibration damping and were used to isolate the different sensors from unwanted vibrations.

3.4.4.1. D435i camera jello effect

Since the jello effect in the RGB + Depth camera was caused by the internal vibrations from the engine, wire rope isolators are expected to be enough to mitigate this problem. Figure 3.21 shows the assembly to be used to isolate the camera from vibrations.

Figure 3.21 - Model of the WRI assembly to be used to reduce the D435i camera jello effect

The difference between isolating or not isolating the camera was unable to be studied so far, so when the vehicle becomes available again, tests should be conducted to verify the effectiveness of WRIs.

3.4.4.2. Duro Inertial isolation

Similarly, the Duro Inertial is affected by the engine's vibrations, which mainly affects its IMU capabilities, as both the accelerometer and gyroscope measurements will contain

some amount of error. When IMU measurements are relied upon to help know the vehicle state, these errors can also accumulate and cause the vehicle state estimate to diverge from the true vehicle state [73].

Following the results obtained in the previous use of wire rope isolators, two different configurations were tested in order to understand which would be more effective in damping vibrations in the three axes, one where all WRIs were mounted at a 45° angle, and one were half were mounted in a vertical position and half were in a horizontal position.

(a) (b)

Figure 3.22 - Different WRIs configurations: (a) 45° configuration, (b) 0°+90° configuration

Table 3.9 shows the comparison of the average acceleration magnitude for all three axes between both proposed configurations and having the Duro Inertial hard mounted.

Table 3.9 - Average acceleration magnitude comparison between each test and Hard Mounted (HM), for all 3 axes

Tests	X axis	Y axis	Z axis
45° / HM	0.17	0.26	0.34
0° + 90° / HM	0.16	0.45	0.39

Both proposed configurations show significant reductions in acceleration magnitudes in all three axes. The 45° configuration shows better damping in the y and z axes with regard to the 0°+90° configuration, whereas the latter is marginally more effective in the x axis. Hence, the 45° configuration is established as the more favourable disposition of wire rope isolators.

The reduction in acceleration magnitudes was not as substantial as the previous use of WRIs in section 3.4.3, which is most likely caused by the wire rope isolators not being properly loaded with the mass of the Duro Inertial alone. The damping system effectiveness

can be improved by either reducing the diameter of the steel cable used, reducing the number of wire rope isolators used, or increasing the isolated mass on top of the dampened structure.

3.5. Sunlight/Darkness

As different lighting conditions occur throughout each day, a complete sensory system is expected to perform differently in differently lit conditions.

If too much light impacts either the stereo depth camera (Intel® RealSense™ D435i) or the multispectral camera (Genie Nano-CL C2420) their respective images will become saturated, also, strong solar radiation can be reflected from some objects, leading to erroneous measurements with the infrared camera. In contrast, neither the LiDAR sensor nor the Duro Inertial will be affected by over-exposure to solar or other light sources.

In a forest environment, the presence of trees and other vegetation will create zones where shadows exist, these shadows can sometimes create errors in sensors measurements, namely in passive sensors.

No experiments were conducted during nighttime, so, sensor behaviour in the absence of light was inferred from the researched state-of-the-art. Without sufficient ambient light present both the stereo depth camera and the multispectral camera will not perform as intended, whereas the remaining sensors will still perform as expected.

If nighttime work is a possible prospect, then higher reliance should be given to the LiDAR sensor, the IR camera, and the Duro Inertial unit, and less to the stereo depth and the multispectral cameras, so as to assure accurate navigation and obstacle avoidance.

3.6. Rain

Due to the inability to operate the machine in the presence of rain, because of the installed components, especially the wiring, not having been assembled to withstand contact with water, no tests were conducted to assess the impact of rain on sensor performance. Nonetheless, the expected influence of this constraint can be analysed through the researched state-of-the-art.

The Duro Inertial is rated for IP67, so it will not be affected by rain. The IR camera used (FLIR ADK) and the LiDAR sensor (Puck) are also IP67-rated, but, even if rain does not affect the sensors' operation, it does affect their measurements, as due to the scattering

of light off water droplets infrared measurements will be affected, and LiDAR accuracy rapidly degrades in heavy mist.

The remaining sensors are not only not rated for use in rainy conditions, but their measurements will also be affected by both falling rain and adherent raindrops. In rainy days, raindrops inevitably adhere to camera lenses, and occlude and deform some image areas, leading to the degradation of traditional algorithms used in sensor-vision applications [74].

If the machine's development advances to the point where operation in the rain can be sustained, then de-raining techniques, such as the ones proposed by Zhang et al. [75] for images, and by Sharma et al. [76] for videos, can be applied and paired with sensor fusion methods, like the one developed by Bijelic et al. [77], to allow the best possible accuracy in rainy environments.

The work developed by Akai et al. [78] also presents possible solutions to the rain challenge. In their developed work, the use of eaves proved enough to greatly reduce rain influence in sensor measurement, this however, came at the cost of more restrictive camera use, and was also less effective for higher wind speeds, where raindrop blowing is more prevalent. Another option is to tilt the cameras to the ground, although this considerably reduces the cameras' actionable angle of view. Both alternatives are aimed at minimizing adherent raindrops on camera lenses, but they do not help with falling rain.

4. RESULTS DISCUSSION

In this chapter the recommendations for the installation of each sensor are summarised, based on the results obtained in the previous chapters. Also, different aspects that were observed throughout the development of this work and that in some way affect the operating conditions of the machine are introduced and possible solutions are discussed.

4.1. Control unit

As no tests were carried out with the NVIDIA Jetson Xavier NX unit, the considerations for the installation of this component are made based only on the constraints analysed.

- The unit should be kept distant from the machine's engine and exhaust, as these are the areas that tend to have the only noteworthy temperature increase;
- As the component is not water-resistant, it should be kept away from any possible contact with water droplets. Alternatively, a waterproof container can be designed to house this, and other components, that do not withstand contact with water. Note that this container would have to be properly designed to correctly cool the components inside, as the temperature ranges of each unit must always be met;
- The unit should be included in the set of components that need to be isolated from vibrations.

4.2. LiDAR sensor

The Puck™ is one of the most reliable sensors considered in this work, as it can perform regardless of lighting conditions and in most environments. Regardless, some guidelines can still be laid out:

- According to the manufacturer, the Puck is rated for IP67, so, even if it can not be immersed in water, it should be protected against powerful water jets. As such, this sensor can be operated in rainy conditions without having to be further protected;

- Although the sensor is impervious to dust, it should still be kept away from areas that have the potential to accumulate more particulates (dust or others), as such particulates can negatively affect LiDAR performance;
- Given its operating capabilities, the Puck should have an unobstructed 360° horizontal field of view and a 30° vertical field of view, in order to fully take advantage of this sensor. This means that the unit should be mounted on a high enough location where no other components cross its field of view, while also assuring it can see the ground;
- As no data was successfully collected to analyse the impact of vibrations on LiDAR measurements it cannot be undoubtedly stated that vibrations will affect the sensor's performance. Nevertheless, it is safe to assume that due to how the sensor operates, rapidly rotating to register 360° measurements, high frequency vibrations can interfere with its working conditions. So, the aim should be to isolate the sensor from vibrations.

4.3. RGB + Depth camera

The Intel® RealSense™ D435i proved ideal to measure distances between the machine and other entities, especially people, which enabled the implementation of reliable safety protocols. However, some of its more restrictive working conditions led to the elaboration of a series of recommendations for the camera's installation:

- Due to its small optimal temperature operating window (0 to 35 °C), if the camera is expected to work in environments with higher temperatures, then proper cooling should be assured to keep the camera working as intended. Covering the camera to avoid direct exposure to sunlight should also be considered;
- As dust can not only penetrated the camera but also affect its measurements when it adheres to the lens, the camera should be mounted on a location not prone to dust accumulation;
- With the aid of the IMU integrated on the camera, video stabilisation is successfully achieved without the need for external additions. However, higher frequency vibrations cause the so-called "jello effect", which considerably

affect image quality, so, the component should be isolated from vibrations as much as possible;

- The camera should not be used at nighttime, as without sufficient ambient light its performance greatly decreases. Likewise, excessive exposure to light sources causes the images to become saturated, so the camera should never be pointed in an upwards direction, as this can quickly lead to saturation due to sun glare;
- As the camera is not suitable for contact with water it should be kept away from any possible contact with water droplets. Alternatively, the already mentioned waterproof container can be used to house this camera as well, always taking into account that proper cooling is of utmost importance.

4.4. Duro Inertial unit

During testing, certain problems with the Duro Inertial unit were encountered which hindered the work being conducted. Consequently, some important guidelines for using this unit, or similar packages that use a GNSS + RTK + IMU system, were delineated, namely:

- Keep the unit as close as possible to the centre of rotation of the machine. Since the GNSS is accurate to a small enough extent, when rotating, if the GNSS receiver is not close to the centre of rotation, then when the vehicle rotates its final coordinates will differ from the initial coordinates. This will then not match with the data from the gyroscope, as the calculations for angular displacement based on the gyroscope measurements assume that rotations are made around the axis that goes through the vehicle's centre;
- Assure an open sky view is possible when the GNSS receiver is first searching for signal. During the conducted tests, the time needed for the receiver to acquire a signal was significantly reduced when a clear view of the sky was available;
- When possible, a direct line of sight to the ground station of the RTK system should be assured. In the forest environment where tests were conducted it was found that RTK connection becomes intermittent when direct light of sight to the ground station is obstructed;

- Always use the same number of decimal places when dealing with coordinates. This GNSS receiver uses coordinates with a precision of 15 decimal places, so if coordinates with less accuracy are transmitted to it, the unit fills in the remaining empty decimal places, which can then direct the robot to the wrong location. Although at first this problem does not constitute a major error, the accumulation of several small inaccuracies can introduce a significant error;
- When an IMU is used to complement the navigation capabilities it should be isolated from vibrations as much as possible, as vibrations tend to induce an error in both accelerometer and gyroscope measurements. However, the IMU should never be stabilised in the rotational space, as this would prevent the gyroscope from sensing when the machine is turning or rotating;
- As the Duro Inertial unit is rated for IP67, it has no problem operating in rainy conditions and in contact with dust and other particulates. Furthermore, since this unit has no lens that can be affect by adherent dust or water, its location is not constrained by external conditions.

If a system where the sensors present in the Duro Inertial are installed as individual units, then the same suggestions should still be followed, howbeit applied to their specific sensors.

4.5. IR camera

As the IR camera considered, the FLIR ADK, was not available during the development of the work, no data is available to evaluate. Even so, some recommendations can still be delineated from the researched state-of-the-art and the constraints analysed.

- Given its IP67 rating, paired with the heated external window, the camera should have no problems operating in all weathers, so no further protection is needed to guarantee sensor performance;
- Due to sun glare, and especially solar radiation reflected from objects, erroneous temperature measurements can be taken. A possible solution to this problem is to use two or more IR cameras, angled differently, so infrared measurements can be confirmed by more than one sensor;

- Contrarily, at nighttime, the camera should work perfectly, as the emissivity of objects is maintained but no solar radiation can affect the measurements;
- As the machine's engine and exhaust have the biggest tendency to heat up, the infrared camera, that measures temperature variations, should not be mounted close to these locations, in order to not influence the sensor's measurements;
- Although no tests were carried out with this camera, it is advisable to isolate it from vibrations when possible.

4.6. Multispectral camera

As the multispectral camera considered, the Genie Nano-CL C2420, was not available during the development of the work, no data is available to evaluate. Even so, some recommendations can still be delineated from the researched state-of-the-art and the constraints analysed.

- Albeit the camera has a wide operating temperature range, it is still recommended to keep it away from areas more prone to high temperatures, i.e., the machine's engine and exhaust;
- Although no tests were carried out with this camera, it is advisable to isolate it from vibrations when possible;
- The remaining recommendations, concerning dust, water, and operation during daytime and nighttime, should be the same as the ones given for the RGB + Depth camera (Intel® RealSense™ D435i).

4.7. Locations for sensor mounting

4.7.1. Use of the mulcher as a sensor platform

Based on the vibration analysis conducted, the mulcher would seem like an ideal place to serve as a platform on which sensors could be mounted. However, other limitations make the mulcher an objectively worse location for sensor mounting, particularly dust accumulation, which was seen as being considerably higher than in other locations on the machine when the tool is in use, also, sensors on mulcher are considerably more at risk of

being damaged by flying branches or similarly displaced vegetation, this is not demonstrated anywhere but was regularly observed when conducting field tests.

4.7.2. Use of the top support as a sensor platform

Although the top support was the location most affected by the internal vibrations generated by the engine (which would be expected, seeing as it is the most eccentric mass in the whole structure) it was also the location least affected by all the remaining constraints, as it is the furthest area from the high temperature zones and the location where the least dust is accumulated. It is also the best location for the installation of the LiDAR sensor, as it allows a clear 360° field of view, and a sensible location for mounting the remaining sensors.

Assuming proper vibration damping can be achieved, the use of an external support to mount a complete sensory system appears to be the best opinion, as it not only provides a safe location to mount sensors and other components but also allows the freedom to create solutions containing an entire sensory system that can fit any machine.

4.8. Set of guidelines

The results and conclusions acquired for the specific sensors tested during the development of this work also enable the elaboration of a broader set of guidelines for the installation of sensory systems on machines inside the scope of field robotics. Such a set is now presented:

- If possible, a gradient of acceleration/deceleration should be introduced to non-emergency situations, in order to avoid sudden shocks being transmitted throughout the machine;
- If a GNSS receiver is employed, it should be kept close to the centre of rotation of the machine and, when possible, open sky conditions should be assured;
- Sensors should not be mounted near the machine's engine, exhaust system, or similar areas that tend to have a high temperature increase when in operation;
- Sensors should be mounted on locations with a safe distance from the working tools of the machine, as in close proximity to said tools dust accumulation is more prevalent and flying debris can damage the sensors;

- For dealing with the high frequencies generated by the machine's engine, wire rope isolators should be considered as one of the most viable solutions. As they not only have a significantly better performance than the other tested solutions but are also easily reproducible with simple manufacturing processes;
- All sensors should be isolated from vibrations as much as possible, as regardless of the extent, all components are affected. However, sensors that deal with the machine's navigation, such as an IMU, should never be isolated in the rotational space;
- As image saturation due to sun glare is a possible issue, the cameras should not be mounted in an upwards angle and, if possible, two or more of the same cameras should be mounted at different angles in order to verify the measurements;
- If nighttime work is an intended requisite of the machine, higher reliance should be given to active sensors, such as IR cameras and LiDAR sensors, that do not lose performance in the absence of light;
- If the machine is intended to operate in rainy conditions, then de-raining techniques, to deal with both falling rain and adherent raindrops, should be applied to minimise accuracy loss. Waterproof containers, or the use of eaves, should also be considered, to protect the sensors;
- Lastly, the use of a singular solution, containing a complete sensory system, should be considered as the most viable alternative, as it allows the easiest application on the machine, and also streamlines the development of vibration damping solutions and protective containers.

5. CONCLUSIONS

The work presented in this dissertation had the goal of validating the use of sensors in a robotic platform as a path to automate the machine's functions in field robotic applications, specifically land clearing and fuelbreak management operations. The final goal was to apply the attained conclusions and delineate a set of recommendations and guidelines that could facilitate the installation of sensory systems in any machine inside the scope of field robotics.

The researched state-of-the-art allowed a deeper understanding of the problems that were expected to be encountered while also focusing the development on solutions that could help mitigate said problems. Subsequently, the tests carried out led to conclusions regarding not only the broader operating capabilities of the machine but also the specific challenges that each constraint presented, which then served as baselines for the recommendations proposed for the installation of each sensor and for the final set of guidelines.

Some limitations and difficulties arose during the work that impaired the progress of the project, namely the lack of access to two of the specified sensors, the IR and multispectral cameras, the beginning of the fire season in Portugal, which restricted the use of the mulcher tool, and some mechanical issues with the machine itself, which limited the number of tests that could be carried out. Also, the impossibility of operating the machine in rainy conditions or at nighttime limited the results obtained.

Overall, the work developed is believed to have contributed to the use of individual sensors and complete sensory systems in robotic applications, being especially beneficial in guiding the installation of said sensors. And even though some constraints were not fully tested (such as performance at night and in the rain), the work is believed to have provided substantial information on how to proceed in the presence of said conditions and the necessary steps to follow for when such constraints can be tested.

5.1. Future work

In the future, more testing is needed to validate the use of the sensors that were not yet available during the duration of this thesis. Additionally, after the machine's development advances to a point where operation in the rain can be sustained, then further tests should be carried out to assess the system's performance in rainy environments. Likewise, if it becomes

possible, experiments should be conducted during nighttime to evaluate the sensors' capabilities in the absence of natural light.

Other complementary work can also be carried out to extend the possible applications of this dissertation, specifically inside the domain of the described wire rope isolators. As the WRIs suggested do not perform the same when used to isolate different components and as it is known that changes in their geometry, wire diameter and disposition will affect their performance, it would be worthwhile to accurately know WRI effectiveness for a specific application, be it through modelling and simulation or through experimental tests.

Similarly, the semi-active tuned mass damper described can be developed and tested so as to understand if an active control system leads to better results in vibration damping for the sensors described. But it could be that its effectiveness is not better than using wire rope isolators, or that the gain in effectiveness does not justify the increased resources needed for a semi-active solution.

Finally, to assure all-weather and all-environment performance of a complete sensory system, sensor fusion should be studied and applied to the system, along with de-raining and other algorithms that extend the applications of said sensory system.

BIBLIOGRAPHY

[1] D. X. Viegas, “O complexo de incêndios de Pedrógão Grande e concelhos limítrofes, iniciado a 17 de junho de 2017,” 2017. [Online]. Available: https://www.portugal.gov.pt/pt/gc21/comunicacao/documento?i=o-complexo-de-incendios-de-pedrogao-grande-e-concelhos-limitrofes-iniciado-a-17-de-junho-de-2017.

[2] ICNF, “Áreas Ardidas.” [Online]. Available: http://www2.icnf.pt/portal/florestas/dfci/inc/cartografia/areas-ardidas.

[3] D. Ascoli, L. Russo, F. Giannino, C. Siettos, and F. Moreira, “Firebreak and Fuelbreak,” in *Encyclopedia of Wildfires and Wildland-Urban Interface (WUI) Fires*, S. L. Manzello, Ed. Cham: Springer International Publishing, 2018, pp. 1–9.

[4] R. Lovreglio, O. Meddour-Sahar, and V. Leone, “Goat grazing as a wildfire prevention tool: a basic review,” *iForest - Biogeosciences For.*, vol. 7, no. 4, pp. 260–268, 2014, doi: 10.3832/ifor1112-007.

[5] E. Kohn, “WILDFIRE LITIGATION,” *Environ. Law*, vol. 48, no. 3, pp. 585–615, Feb. 2018, [Online]. Available: http://www.jstor.org/stable/26507763.

[6] MDB Technologies, “Green Climber LV400.” https://www.mdbsrl.com/lv-400/ (accessed Jan. 25, 2022).

[7] SME Mowers, “Green Climber LV400 Pro,” 2021. https://greenclimber.com.au/mowers/green-climber-lv400-pro/ (accessed Jan. 28, 2022).

[8] NVIDIA Corporation, “Jetson Xavier NX Series.” https://www.nvidia.com/en-us/autonomous-machines/embedded-systems/jetson-xavier-nx/ (accessed Jan. 26, 2022).

[9] International Electrotechnical Commission, “IP Ratings.” https://www.iec.ch/ip-ratings (accessed Jun. 26, 2022).

[10] A. Ullrich, “Sampling the World in 3D by Airborne LIDAR – Assessing the Information Content of LIDAR Point Clouds,” *Photogramm. Week 2013*, pp. 247–259, 2013, [Online]. Available: https://phowo.ifp.uni-stuttgart.de/publications/phowo13/210Ullrich.pdf.

[11] D. M. Aubrecht, B. R. Helliker, M. L. Goulden, D. A. Roberts, C. J. Still, and A. D. Richardson, “Continuous, long-term, high-frequency thermal imaging of vegetation: Uncertainties and recommended best practices,” *Agric. For. Meteorol.*, vol. 228–229, pp. 315–326, 2016, doi: https://doi.org/10.1016/j.agrformet.2016.07.017.

[12] M. Litwa, “Influence of Angle of View on Temperature Measurements Using Thermovision Camera,” *IEEE Sens. J.*, vol. 10, no. 10, pp. 1552–1554, 2010, doi: 10.1109/JSEN.2010.2045651.

[13] Fecon, “125VRT Mulching Tractor,” 2021. https://yellow.fecon.com/product/125vrt/ (accessed Dec. 28, 2021).

[14] MDB Technologies, “Green Climber,” 2018. https://www.mdbsrl.com/greenclimber/ (accessed Dec. 28, 2021).

[15] L. F. P. Oliveira, A. P. Moreira, and M. F. Silva, “Advances in forest robotics: A state-of-the-art survey,” *Robotics*, vol. 10, no. 2, pp. 1–20, 2021, doi: 10.3390/robotics10020053.

[16] Q. Li, P. Nevalainen, J. P. Queralta, J. Heikkonen, and T. Westerlund, “Localization in unstructured environments: Towards autonomous robots in forests with Delaunay triangulation,” *Remote Sens.*, vol. 12, no. 11, 2020, doi: 10.3390/rs12111870.
[17] A. K. Nasir, A. G. Araújo, and M. S. Couceiro, “Localization and navigation assessment of a heavy-duty field robot,” in *Proceedings of the 2020 IEEE/RSJ International Conference on Intelligent Robots and Systems (IROS 2020), Workshop on Perception, Planning and Mobility in Forestry Robotics (WPPMFR 2020)*, 2020, pp. 25–29.
[18] R. G. D’Eon, R. Serrouya, G. Smith, and C. O. Kochanny, “GPS Radiotelemetry Error and Bias in Mountainous Terrain,” *Wildl. Soc. Bull.*, vol. 30, no. 2, pp. 430–439, Dec. 2002, [Online]. Available: http://www.jstor.org/stable/3784501.
[19] A. S. Aguiar, F. N. Dos Santos, J. B. Cunha, H. Sobreira, and A. J. Sousa, “Localization and mapping for robots in agriculture and forestry: A survey,” *Robotics*, vol. 9, no. 4, pp. 1–23, 2020, doi: 10.3390/robotics9040097.
[20] F. Hardarson, *Locomotion for difficult terrain*. Citeseer, 1998.
[21] Shark Robotics, “Colossus,” 2020. https://www.shark-robotics.com/shark-robots (accessed Dec. 29, 2021).
[22] Milrem Robotics, “Multiscope Rescue with Hydra,” 2020. https://milremrobotics.com/product/multiscope-rescue-hydra/ (accessed Dec. 29, 2021).
[23] Fire Apparatus, “Firefighting Robotic Vehicle System,” 2020. https://www.fireapparatusmagazine.com/fire-apparatus/firefighting-robotic-vehicle-system/ (accessed Dec. 29, 2021).
[24] V. Partel, L. Costa, and Y. Ampatzidis, “Smart tree crop sprayer utilizing sensor fusion and artificial intelligence,” *Comput. Electron. Agric.*, vol. 191, p. 106556, 2021, doi: 10.1016/j.compag.2021.106556.
[25] S. Birrell, J. Hughes, and J. Y. Cai, “A field - tested robotic harvesting system for iceberg lettuce,” no. August 2018, pp. 225–245, 2020, doi: 10.1002/rob.21888.
[26] G. Freitas, F. Lizarralde, L. Hsu, and N. R. S. Dos Reis, “Kinematic reconfigurability of mobile robots on irregular terrains,” *Proc. - IEEE Int. Conf. Robot. Autom.*, pp. 1340–1345, 2009, doi: 10.1109/ROBOT.2009.5152309.
[27] J. Sandino, G. Pegg, F. Gonzalez, and G. Smith, “Aerial mapping of forests affected by pathogens using UAVs, hyperspectral sensors, and artificial intelligence,” *Sensors (Switzerland)*, vol. 18, no. 4, pp. 1–17, 2018, doi: 10.3390/s18040944.
[28] L. F. Gonzalez, G. A. Montes, E. Puig, S. Johnson, K. Mengersen, and K. J. Gaston, “Unmanned aerial vehicles (UAVs) and artificial intelligence revolutionizing wildlife monitoring and conservation,” *Sensors (Switzerland)*, vol. 16, no. 1, 2016, doi: 10.3390/s16010097.
[29] S. W. Chen *et al.*, “SLOAM: Semantic Lidar Odometry and Mapping for Forest Inventory,” *IEEE Robot. Autom. Lett.*, vol. 5, no. 2, pp. 612–619, 2020, doi: 10.1109/LRA.2019.2963823.
[30] M. S. Couceiro, D. Portugal, J. F. Ferreira, and R. P. Rocha, “SEMFIRE: Towards a new generation of forestry maintenance multi-robot systems,” *Proc. 2019 IEEE/SICE Int. Symp. Syst. Integr. SII 2019*, pp. 270–276, 2019, doi: 10.1109/SII.2019.8700403.
[31] R. Reis, F. N. dos Santos, and L. Santos, “Forest Robot and Datasets for Biomass Collection,” in *Robot 2019: Fourth Iberian Robotics Conference*, 2020, pp. 152–163.

[32] H. Mahdisoozani *et al.*, “Performance enhancement of internal combustion engines through vibration control: State of the art and challenges,” *Appl. Sci.*, vol. 9, no. 3, 2019, doi: 10.3390/app9030406.
[33] T. Ramachandran and K. P. Padmanaban, “Review on internal combustion engine vibrations and mountings,” *Int. J. Eng. Sci. \& Emerg. Technol.*, vol. 3, no. 1, pp. 63–73, 2012.
[34] H. Ç. SEZGEN and M. TINKIR, “Optimization of torsional vibration damper of cranktrain system using a hybrid damping approach,” *Eng. Sci. Technol. an Int. J.*, vol. 24, no. 4, pp. 959–973, 2021, doi: https://doi.org/10.1016/j.jestch.2021.02.008.
[35] T. Yuvapriya, P. Lakshmi, and S. Rajendiran, “Vibration suppression in full car active suspension system using fractional order sliding mode controller,” *J. Brazilian Soc. Mech. Sci. Eng.*, vol. 40, no. 4, p. 217, 2018, doi: 10.1007/s40430-018-1138-0.
[36] D. F. Ledezma-Ramírez, P. E. Tapia-González, N. Ferguson, M. Brennan, and B. Tang, “Recent Advances in Shock Vibration Isolation: An Overview and Future Possibilities,” *Appl. Mech. Rev.*, vol. 71, no. 6, Sep. 2019, doi: 10.1115/1.4044190.
[37] norelem, “Compression springs.” https://norelem.co.uk/en/Machine-and-plant-construction/26000/Springs/Compression-springs-ISO-10243-moderate-load/p/agid.20048 (accessed Jan. 20, 2022).
[38] KIPP, “Rubber Buffers.” https://www.kippusa.com/us/en/Products/Rubber-Buffers.html (accessed Jan. 20, 2022).
[39] A. M. Baz, *Active and passive vibration damping*. John Wiley \& Sons, 2019.
[40] norelem, “Damping plates.” https://norelem.co.uk/en/Machine-and-plant-construction/26000/Damping-plates/Damping-plates/p/agid.22817 (accessed Jan. 20, 2022).
[41] D. Shah, G. Metta, and A. Parmiggiani, “Comparison of Workspace Analysis for Different Spherical Parallel Mechanisms: Proceedings of the 4th IFToMM Symposium on Mechanism Design for Robotics,” 2019, pp. 193–201.
[42] P. S. Balaji, M. Rahman, M. Leblouba, and H. H. Lau, “Wire rope isolators for vibration isolation of equipment and structures – A review,” *IOP Conf. Ser. Mater. Sci. Eng.*, vol. 78, Apr. 2015, doi: 10.1088/1757-899X/78/1/012001.
[43] Socitec, “Wire Rope Isolators.” https://socitec.com/en/our-products/wire-rope-isolators/ (accessed Jan. 20, 2022).
[44] Socitec, “Polycal wire rope isolators.” https://socitec.com/en/products/polycal-wire-rope-isolators/ (accessed Jan. 20, 2022).
[45] Vibrostop, “AVAU HF.” https://www.vibrostop.it/en/product/wire-rope-isolators/avau-hf/ (accessed Jan. 20, 2022).
[46] J. V. T. Arias, P. J. L. Eguia, N. T. H., C. Z. M. Lacorte, and A. L. P. de Ocampo, “Gyroscopic Stabilizer for 3D Mapping Device on Unmanned Ground Vehicle,” in *TENCON 2018 - 2018 IEEE Region 10 Conference*, 2018, pp. 2395–2398, doi: 10.1109/TENCON.2018.8650057.
[47] C. Weiss, H. Frohlich, and A. Zell, “Vibration-based Terrain Classification Using Support Vector Machines,” in *2006 IEEE/RSJ International Conference on Intelligent Robots and Systems*, 2006, pp. 4429–4434, doi: 10.1109/IROS.2006.282076.
[48] M. Mei, J. Chang, Y. Li, Z. Li, X. Li, and W. Lv, “Comparative Study of Different Methods in Vibration-Based Terrain Classification for Wheeled Robots with Shock Absorbers,” *Sensors*, vol. 19, no. 5, 2019, doi: 10.3390/s19051137.

[49] H. El-Kebir, T. Shafa, A. Purushottam, M. Ornik, and A. Soylemezoglu, “High-Frequency Vibration Reduction for Unmanned Ground Vehicles on Unstructured Terrain,” *8th Int. Conf. Model. Simul. Auton. Syst.*, 2021, [Online]. Available: https://mornik.web.illinois.edu/wp-content/uploads/ESPOS21.pdf.
[50] C. Spelta *et al.*, “Performance analysis of semi-active suspensions with control of variable damping and stiffness,” *Veh. Syst. Dyn.*, vol. 49, no. 1–2, pp. 237–256, 2011, doi: 10.1080/00423110903410526.
[51] Y. Xu, M. Ahmadian, and R. Sun, “Improving Vehicle Lateral Stability Based on Variable Stiffness and Damping Suspension System via MR Damper,” *IEEE Trans. Veh. Technol.*, vol. 63, no. 3, pp. 1071–1078, 2014, doi: 10.1109/TVT.2013.2282824.
[52] G. J. Liao, X.-L. Gong, S. H. Xuan, C. J. Kang, and L. H. Zong, “Development of a real-time tunable stiffness and damping vibration isolator based on magnetorheological elastomer,” *J. Intell. Mater. Syst. Struct.*, vol. 23, no. 1, pp. 25–33, 2012, doi: 10.1177/1045389X11429853.
[53] S. Sun *et al.*, “A New Generation of Magnetorheological Vehicle Suspension System With Tunable Stiffness and Damping Characteristics,” *IEEE Trans. Ind. Informatics*, vol. 15, no. 8, pp. 4696–4708, 2019, doi: 10.1109/TII.2018.2890290.
[54] T. G. Phillips, N. Guenther, and P. R. McAree, “When the Dust Settles: The Four Behaviors of LiDAR in the Presence of Fine Airborne Particulates,” *J. F. Robot.*, vol. 34, no. 5, pp. 985–1009, 2017, doi: https://doi.org/10.1002/rob.21701.
[55] J. Ryde and N. Hillier, “Performance of laser and radar ranging devices in adverse environmental conditions,” *J. F. Robot.*, vol. 26, no. 9, pp. 712–727, Sep. 2009, doi: https://doi.org/10.1002/rob.20310.
[56] Teledyne FLIR, “Can Thermal Imaging See Through Fog and Rain?,” 2020. https://www.flir.com/discover/rd-science/can-thermal-imaging-see-through-fog-and-rain/ (accessed Feb. 09, 2022).
[57] J. W. Starr and B. Y. Lattimer, “Evaluation of Navigation Sensors in Fire Smoke Environments,” *Fire Technol.*, vol. 50, no. 6, pp. 1459–1481, 2014, doi: 10.1007/s10694-013-0356-3.
[58] J. Pascoal, L. Marques, and A. T. de Almeida, “Assessment of Laser Range Finders in risky environments,” in *2008 IEEE/RSJ International Conference on Intelligent Robots and Systems*, 2008, pp. 3533–3538, doi: 10.1109/IROS.2008.4650961.
[59] D. Pan, Z. Jiang, W. Gui, X. Maldague, and K. Jiang, “Influence of Dust on Temperature Measurement Using Infrared Thermal Imager,” *IEEE Sens. J.*, vol. 20, no. 6, pp. 2911–2918, 2020, doi: 10.1109/JSEN.2019.2957064.
[60] K. Yoneda, N. Suganuma, R. Yanase, and M. Aldibaja, “Automated driving recognition technologies for adverse weather conditions,” *IATSS Res.*, vol. 43, no. 4, pp. 253–262, 2019, doi: https://doi.org/10.1016/j.iatssr.2019.11.005.
[61] H. Madura, M. Kastek, T. Sosnowski, and T. Orżanowski, “Pyrometric Method of Temperature Measurement with Compensation for Solar Radiation,” *Metrology and Measurement Systems*, no. 1. p. 77, 2010, doi: 10.2478/v10178-010-0008-6.
[62] H. Madura and M. Kołodziejczyk, “Influence of sun radiation on results of non-contact temperature measurements in far infrared range,” *Opto-Electronics Rev.*, vol. 13, no. 3, pp. 253–257, 2005.
[63] N. Pinchon *et al.*, “All-Weather Vision for Automotive Safety: Which Spectral Band?,” in *Advanced Microsystems for Automotive Applications 2018*, 2019, pp. 3–15.

[64] Y. Cai, E. Lam, T. Howlett, and A. Cai, "Spatiotemporal Analysis of 'Jello Effect' in Drone Videos," in *Advances in Human Factors in Robots and Unmanned Systems*, 2020, pp. 197–207.
[65] Teledyne FLIR, "FLIR T1020." https://www.flir.com/products/t1020/ (accessed Jun. 10, 2022).
[66] "Hex Cube Black Flight Controller." https://docs.px4.io/master/en/flight_controller/pixhawk-2.html (accessed Jun. 12, 2022).
[67] C. E. Shannon, "Communication in the Presence of Noise," *Proc. IRE*, vol. 37, no. 1, pp. 10–21, 1949, doi: 10.1109/JRPROC.1949.232969.
[68] MathWorks, "Fast Fourier transform." https://www.mathworks.com/help/matlab/ref/fft.html (accessed Jul. 07, 2022).
[69] S. S. Rao, "Vibration Control," in *Mechanical Vibrations*, Pearson, 2018, pp. 819–923.
[70] B. Fitzgerald, S. Sarkar, and A. Staino, "Improved reliability of wind turbine towers with active tuned mass dampers (ATMDs)," *J. Sound Vib.*, vol. 419, pp. 103–122, 2018, doi: https://doi.org/10.1016/j.jsv.2017.12.026.
[71] M. Maślanka, "Optimised semi-active tuned mass damper with acceleration and relative motion feedbacks," *Mech. Syst. Signal Process.*, vol. 130, pp. 707–731, 2019, doi: https://doi.org/10.1016/j.ymssp.2019.05.025.
[72] Nature3D, "Elastic Filaments." https://www.nature3d.com/special/detail/Elastic?id=19 (accessed May 03, 2022).
[73] J. A. Farrell, F. O. Silva, F. Rahman, and J. Wendel, "IMU Error Modeling Tutorial: INS state estimation with real-time sensor calibration," 2021. [Online]. Available: https://escholarship.org/uc/item/1vf7j52p.
[74] S. You, R. T. Tan, R. Kawakami, Y. Mukaigawa, and K. Ikeuchi, "Adherent Raindrop Modeling, Detection and Removal in Video," *IEEE Trans. Pattern Anal. Mach. Intell.*, vol. 38, no. 9, pp. 1721–1733, 2016, doi: 10.1109/TPAMI.2015.2491937.
[75] H. Zhang, V. Sindagi, and V. M. Patel, "Image De-Raining Using a Conditional Generative Adversarial Network," *IEEE Trans. Circuits Syst. Video Technol.*, vol. 30, no. 11, pp. 3943–3956, 2020, doi: 10.1109/TCSVT.2019.2920407.
[76] P. K. Sharma, S. Ghosh, and A. Sur, "High-Quality Frame Recurrent Video De-Raining with Multi-Contextual Adversarial Network," *ACM Trans. Multimed. Comput. Commun. Appl.*, vol. 17, no. 2, May 2021, doi: 10.1145/3444974.
[77] M. Bijelic *et al.*, "Seeing Through Fog Without Seeing Fog: Deep Multimodal Sensor Fusion in Unseen Adverse Weather," Jun. 2020.
[78] N. Akai, Y. Kakigi, S. Yoneyama, and K. Ozaki, "Development of Autonomous Mobile Robot that Can Navigate in Rainy Situations," *J. Robot. Mechatronics*, vol. 28, no. 4, pp. 441–450, 2016, doi: 10.20965/jrm.2016.p0441.

APPENDIX A – RESULTS FOR DUST ACCUMULATION

A1. Dust accumulation without the use of the mulcher tool

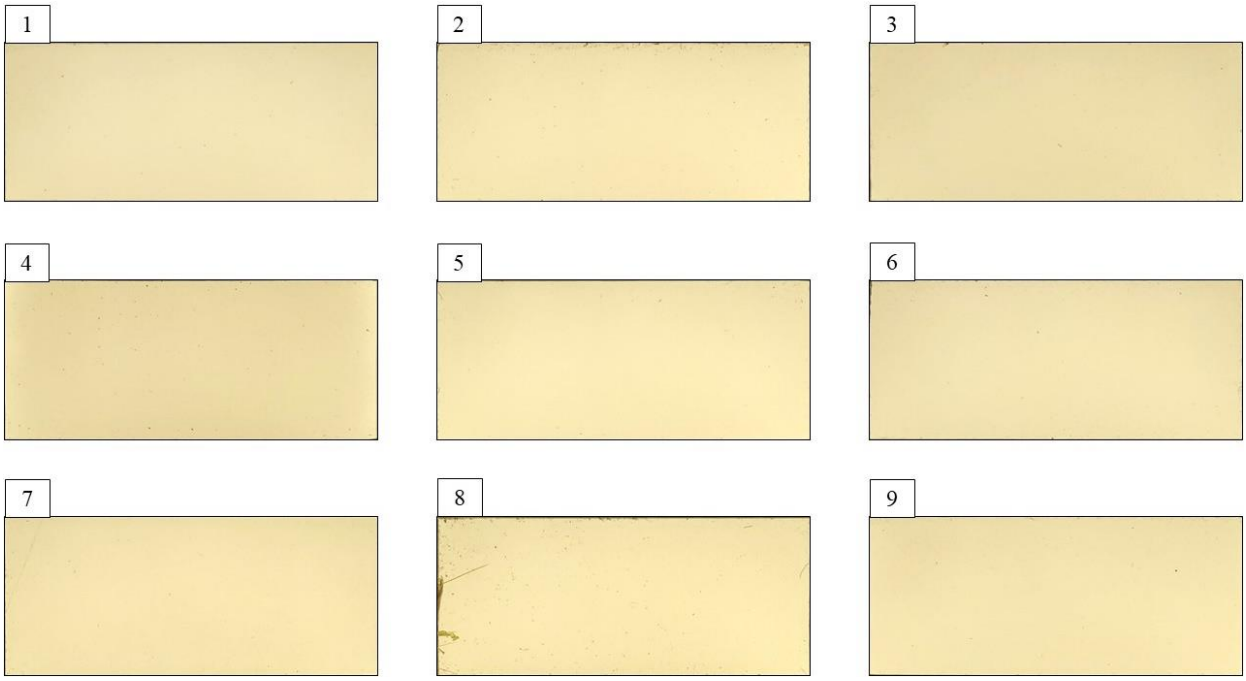

A2. Dust accumulation with the use of the mulcher tool

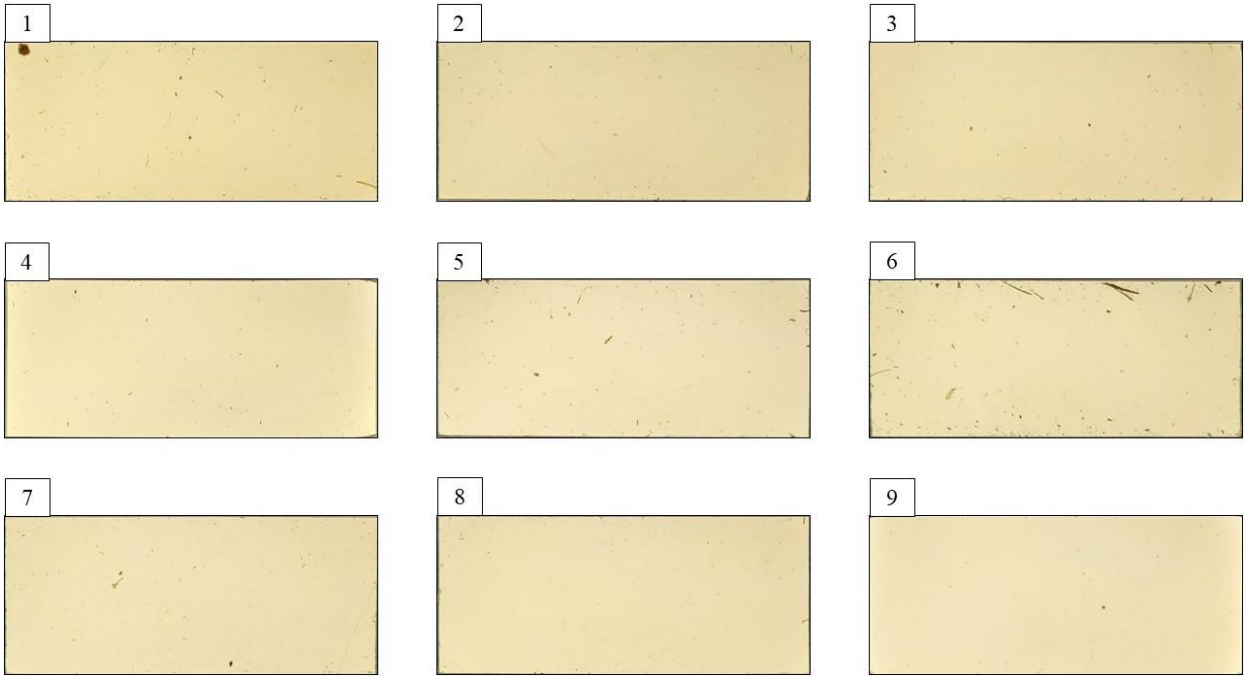

APPENDIX B – VIBRATION DATA FOR ALL TESTS CONDUCTED

B1. Tests for different locations on the machine

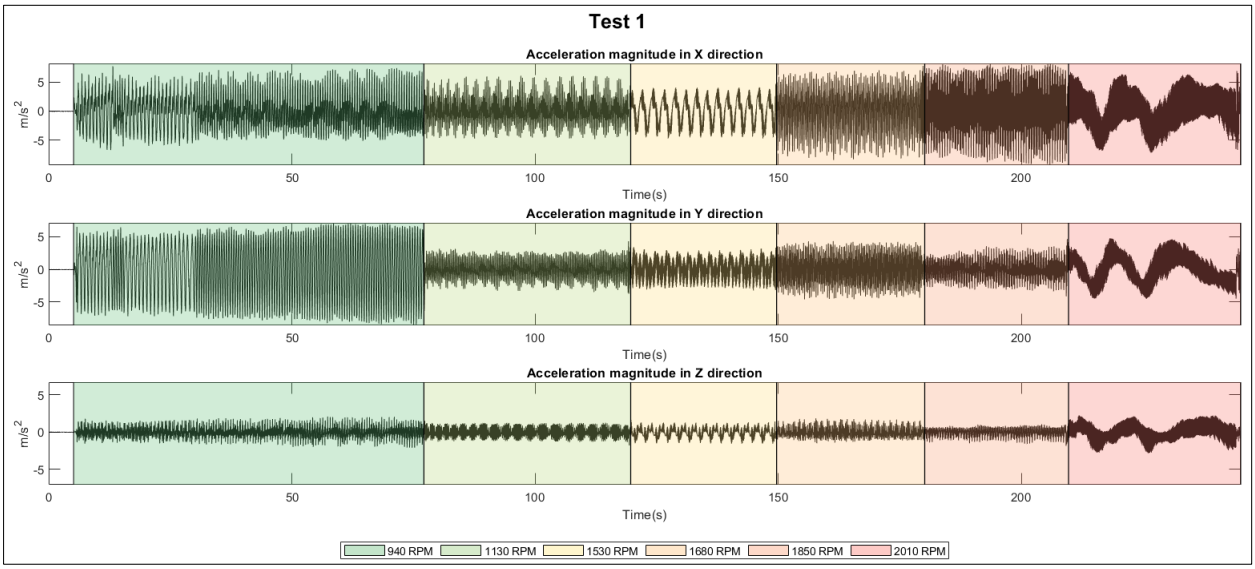

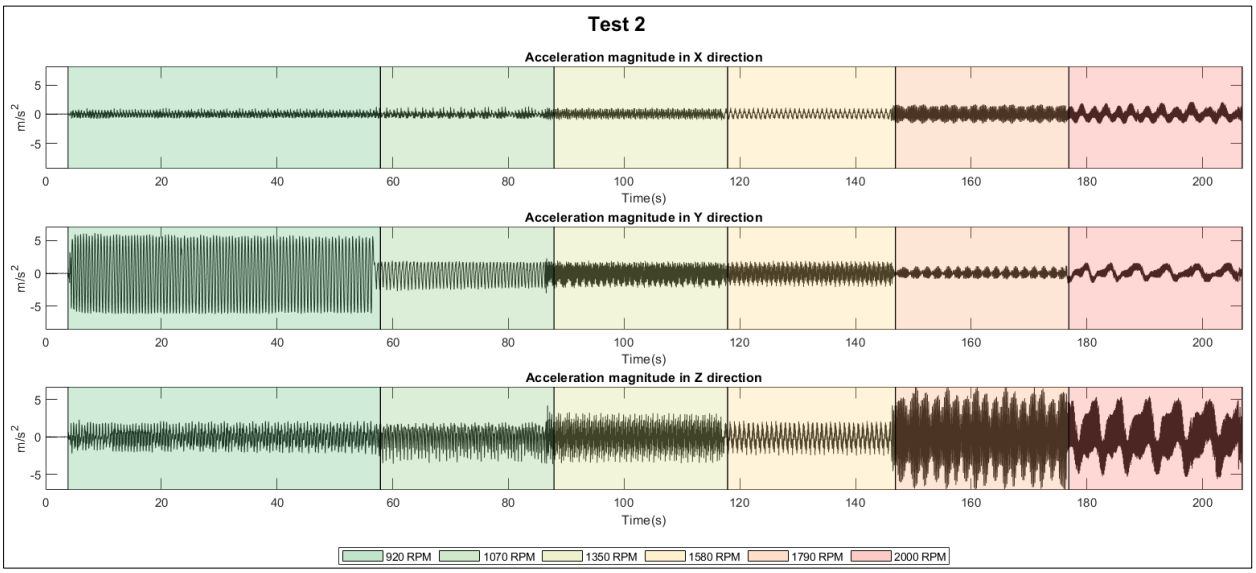

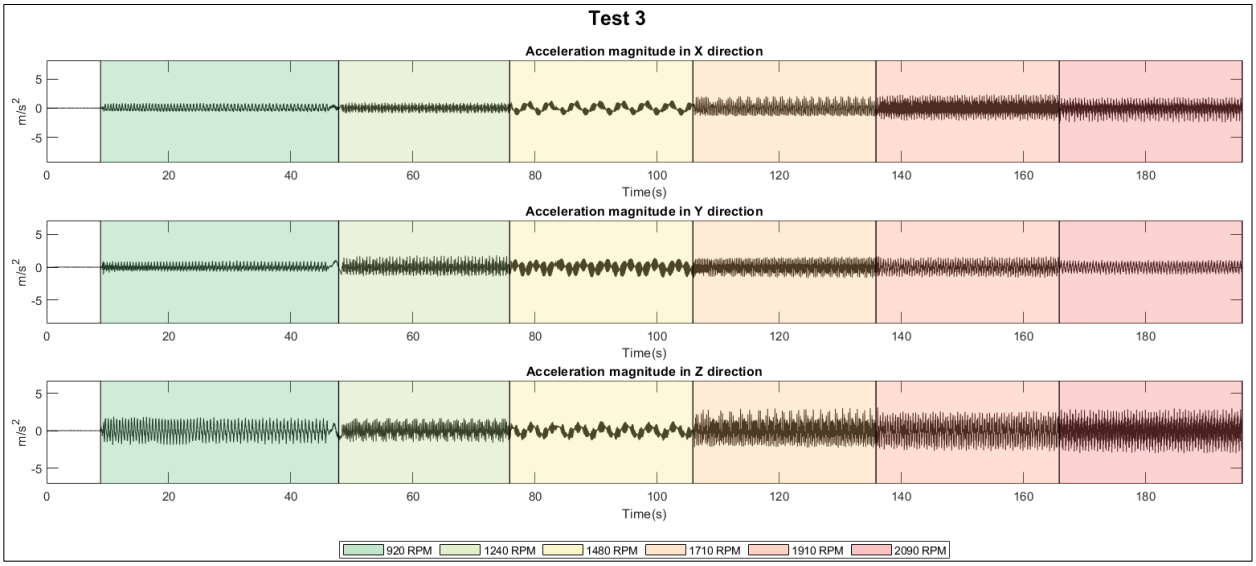
Test 3
Acceleration magnitude in X direction
Acceleration magnitude in Y direction
Acceleration magnitude in Z direction
m/s2
Time(s)
920 RPM
1240 RPM
1480 RPM
1710 RPM
1910 RPM
2090 RPM

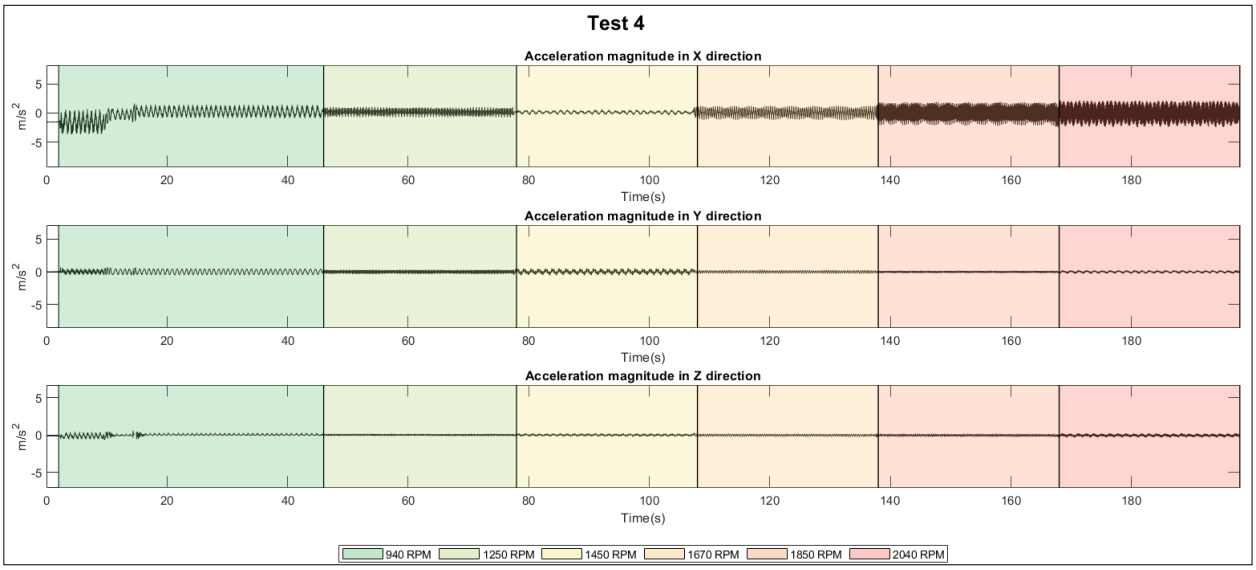
Test 4
Acceleration magnitude in X direction
Acceleration magnitude in Y direction
Acceleration magnitude in Z direction
m/s2
Time(s)
940 RPM
1250 RPM
1450 RPM
1670 RPM
1850 RPM
2040 RPM

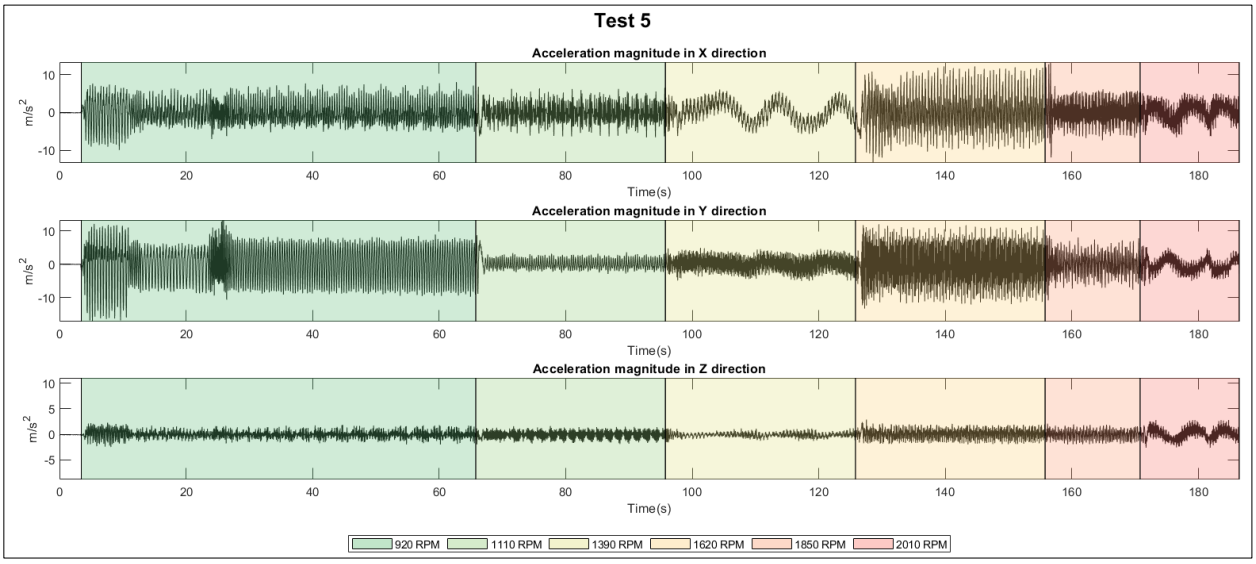
Test 5
Acceleration magnitude in X direction
Acceleration magnitude in Y direction
Acceleration magnitude in Z direction
m/s2
Time(s)
920 RPM
1110 RPM
1390 RPM
1620 RPM
1850 RPM
2010 RPM

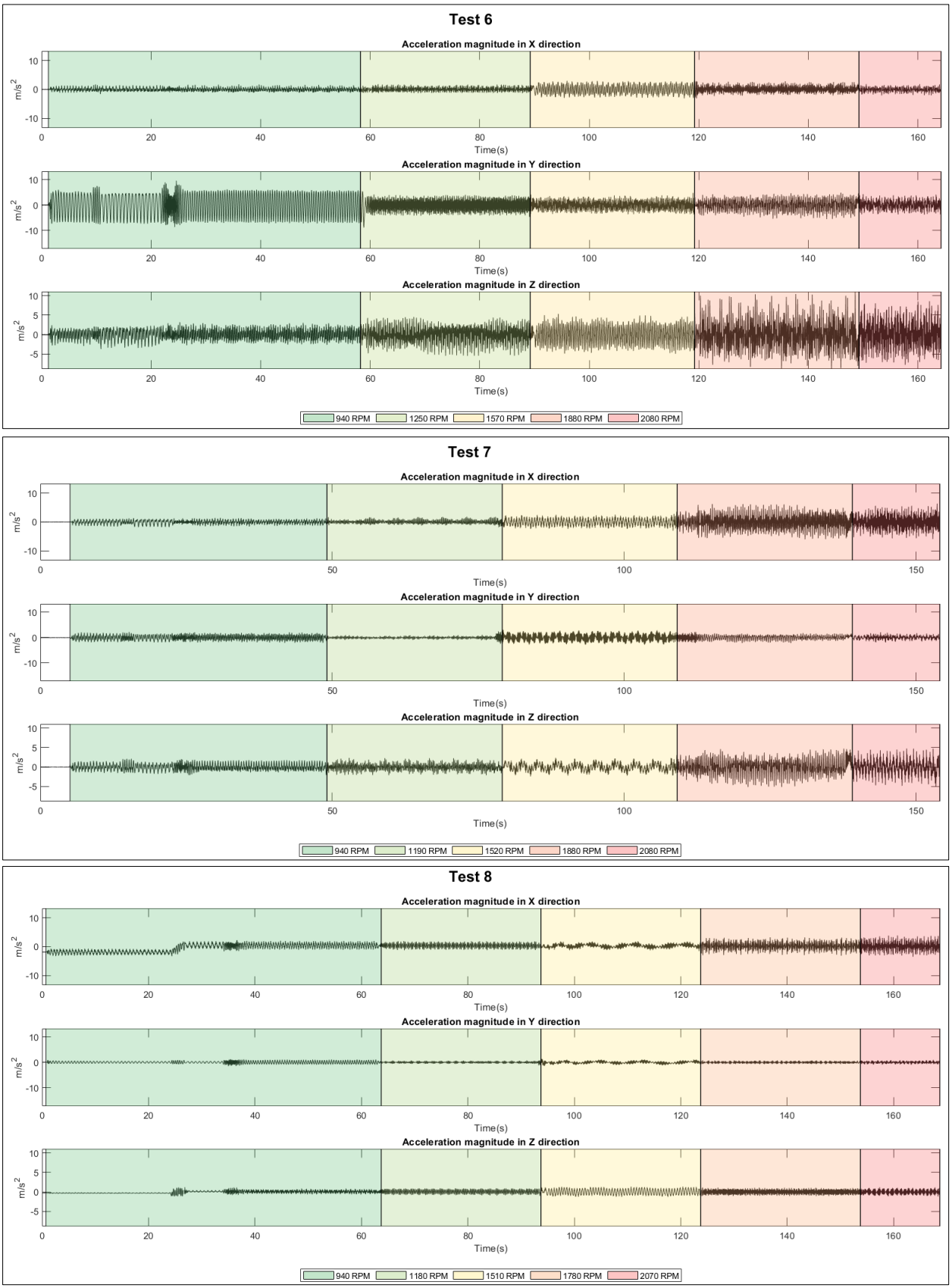
Test 6
Acceleration magnitude in X direction
Acceleration magnitude in Y direction
Acceleration magnitude in Z direction
m/s^2
Time(s)
940 RPM
1250 RPM
1570 RPM
1880 RPM
2080 RPM
Test 7
Acceleration magnitude in X direction
Acceleration magnitude in Y direction
Acceleration magnitude in Z direction
m/s^2
Time(s)
940 RPM
1190 RPM
1520 RPM
1880 RPM
2080 RPM
Test 8
Acceleration magnitude in X direction
Acceleration magnitude in Y direction
Acceleration magnitude in Z direction
m/s^2
Time(s)
940 RPM
1180 RPM
1510 RPM
1780 RPM
2070 RPM

B2. Tests for different solutions for vibration damping

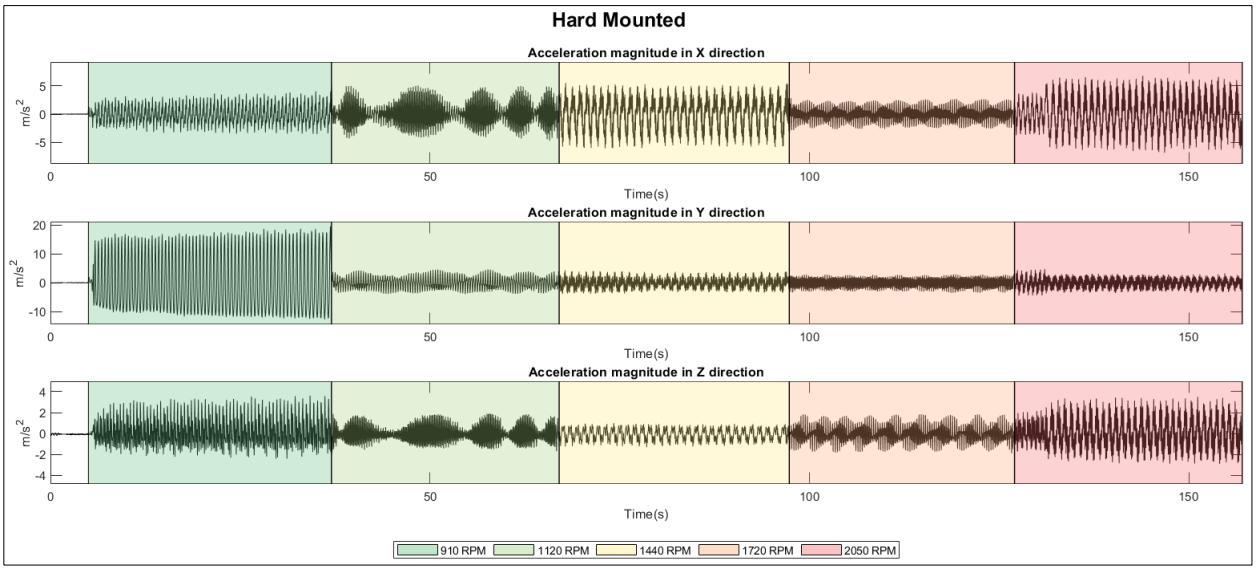

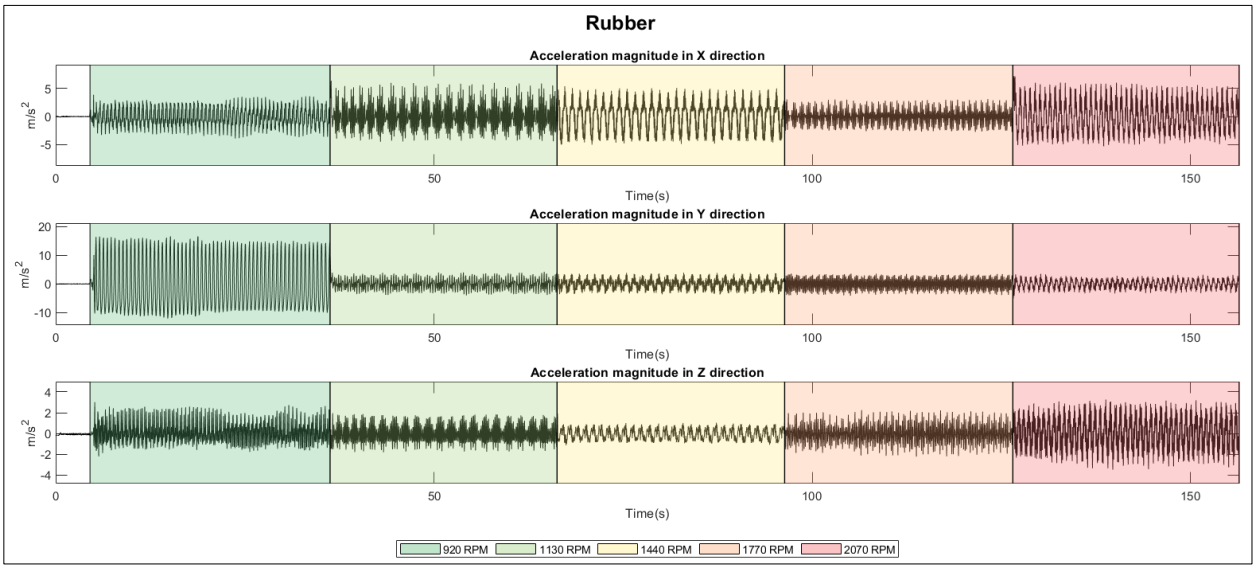

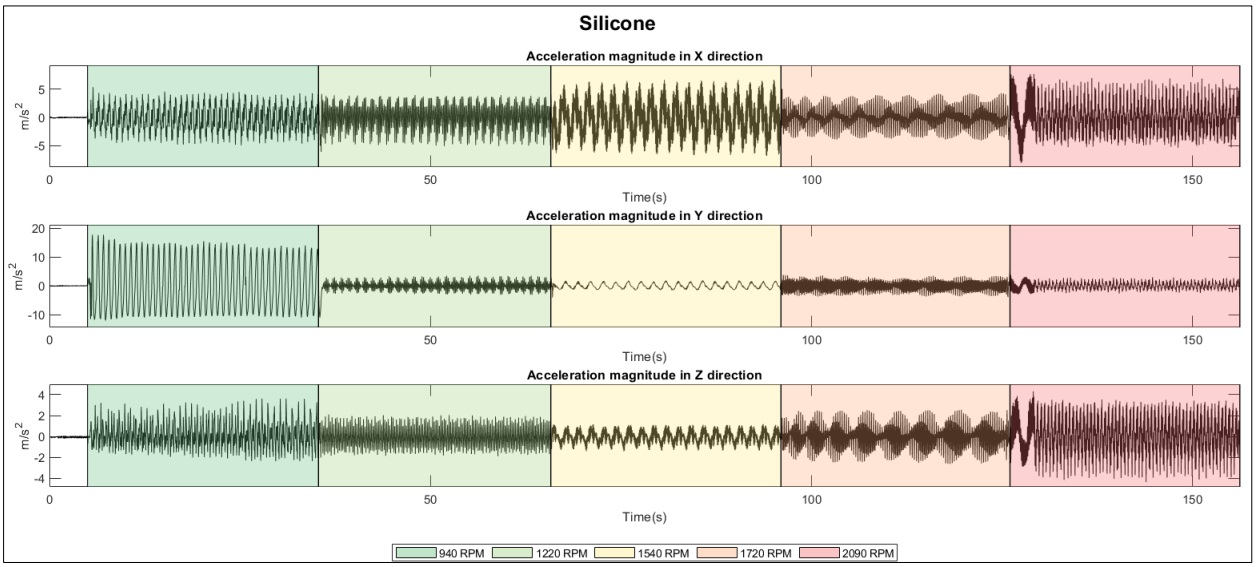
Silicone
Acceleration magnitude in X direction
Acceleration magnitude in Y direction
Acceleration magnitude in Z direction
m/s^2
Time(s)
940 RPM
1220 RPM
1540 RPM
1720 RPM
2090 RPM

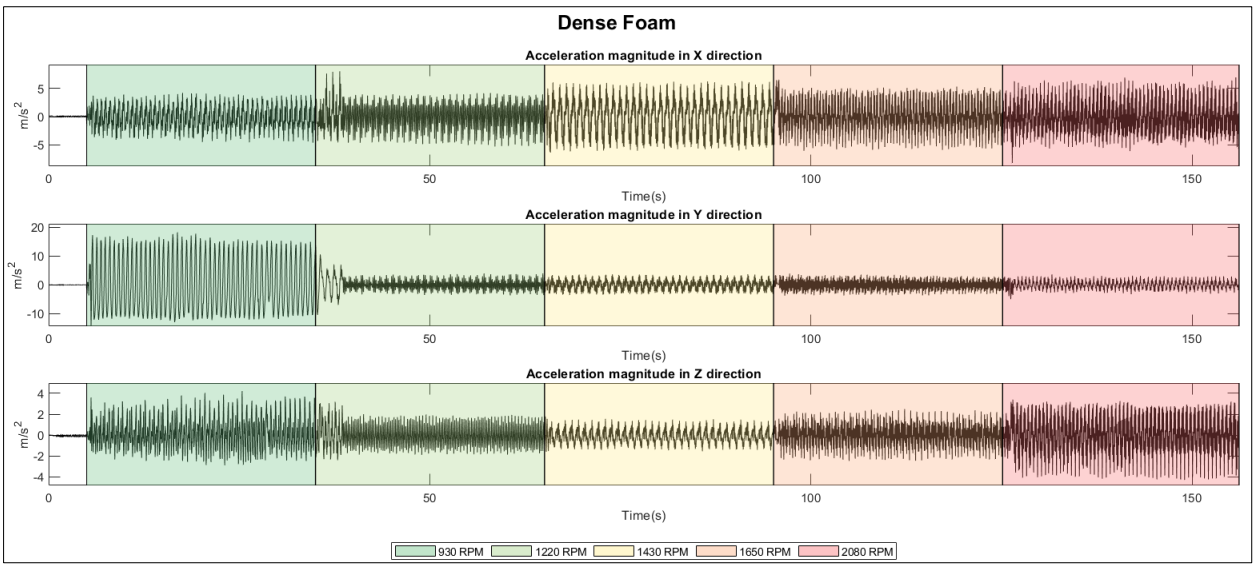
Dense Foam
Acceleration magnitude in X direction
Acceleration magnitude in Y direction
Acceleration magnitude in Z direction
m/s^2
Time(s)
930 RPM
1220 RPM
1430 RPM
1650 RPM
2080 RPM

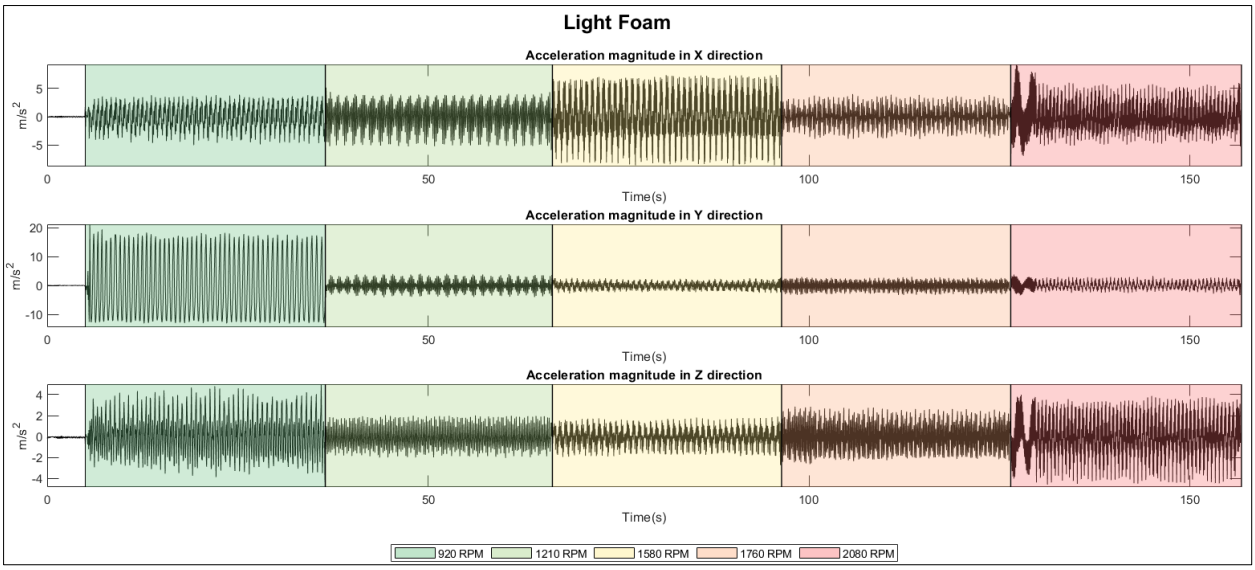
Light Foam
Acceleration magnitude in X direction
Acceleration magnitude in Y direction
Acceleration magnitude in Z direction
m/s^2
Time(s)
920 RPM
1210 RPM
1580 RPM
1760 RPM
2080 RPM

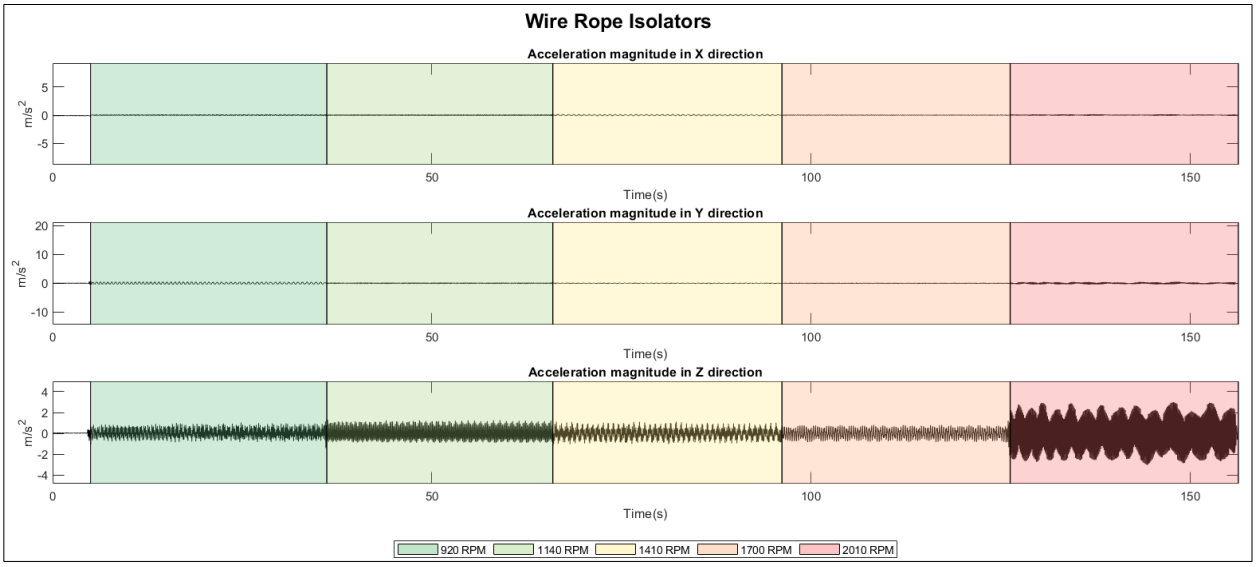

B3. Duro Inertial isolation

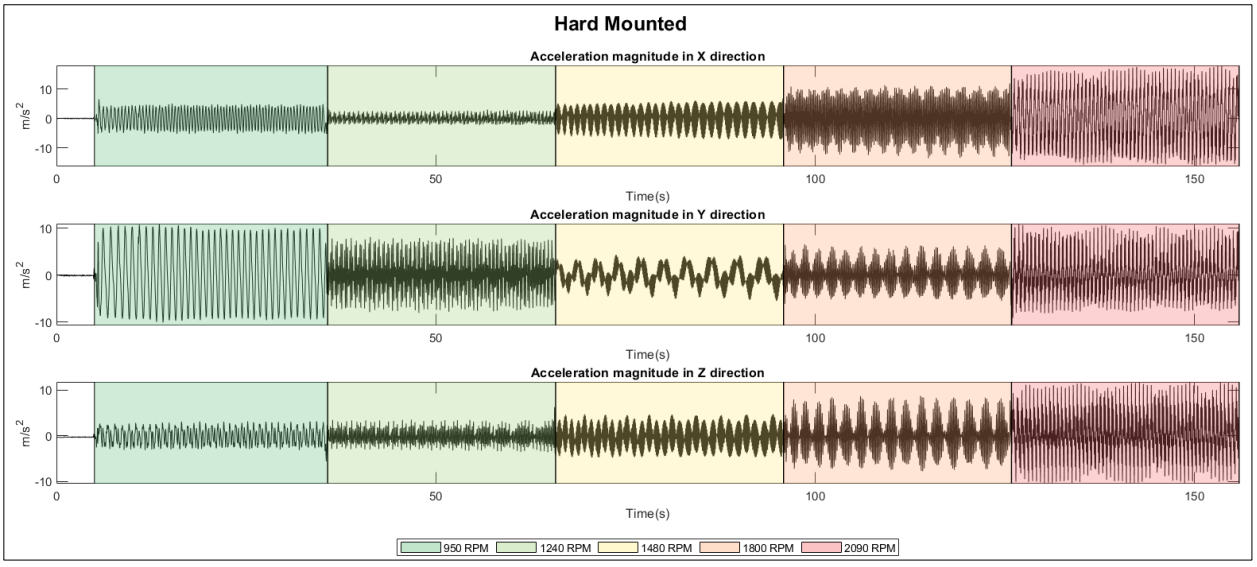

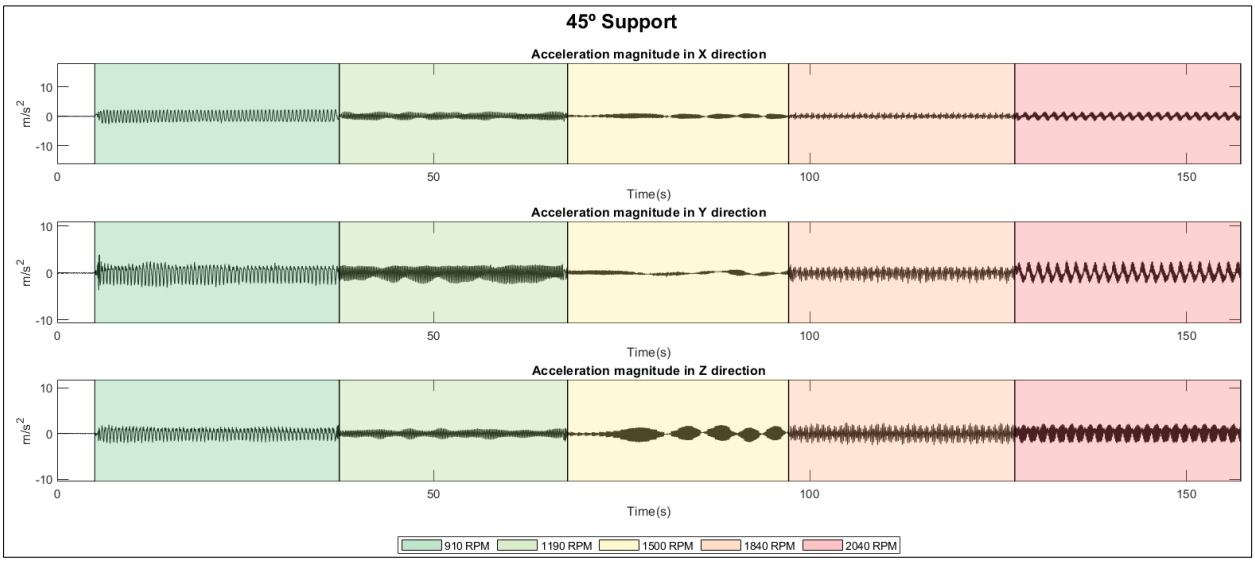
45º Support
Acceleration magnitude in X direction
Acceleration magnitude in Y direction
Acceleration magnitude in Z direction
m/s^2
Time(s)
910 RPM
1190 RPM
1500 RPM
1840 RPM
2040 RPM

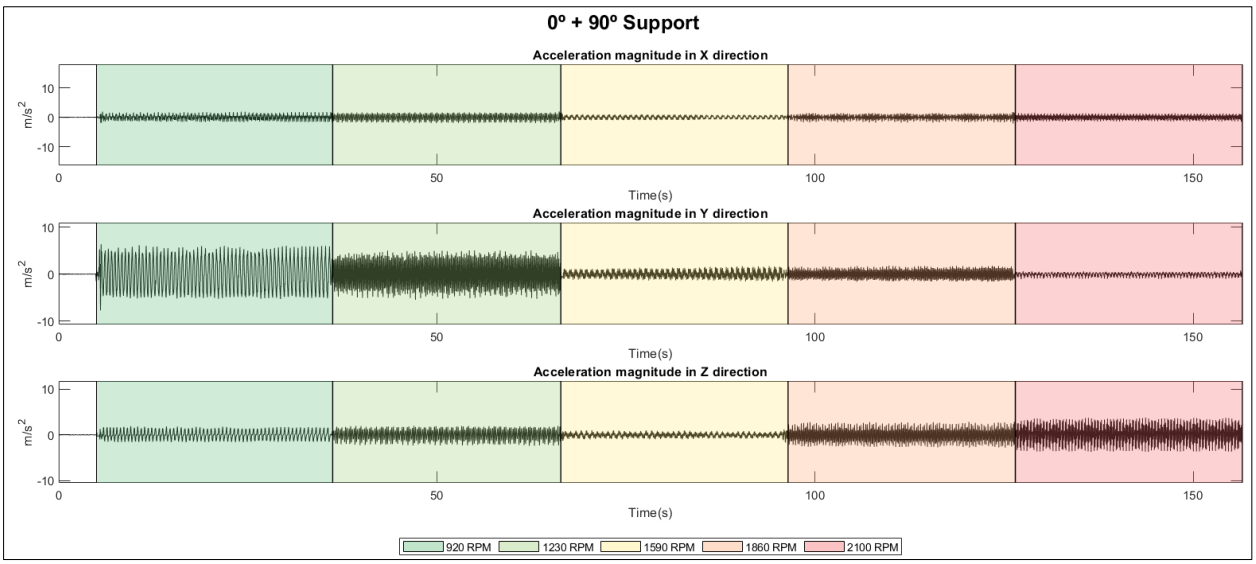
0º + 90º Support
Acceleration magnitude in X direction
Acceleration magnitude in Y direction
Acceleration magnitude in Z direction
m/s^2
Time(s)
920 RPM
1230 RPM
1590 RPM
1860 RPM
2100 RPM

APPENDIX C – AVERAGE ACCELERATION MAGNITUDE FOR ALL VIBRATION TESTS CONDUCTED

All values are in m/s^2.

C1. Tests for different locations on the machine

Test nº	X axis	Y axis	Z axis
1	2.697	2.274	0.638
2	0.500	1.596	1.613
3	0.616	0.562	0.864
4	0.725	0.174	0.104
5	2.743	3.505	0.661
6	0.754	2.588	1.978
7	1.121	0.770	0.947
8	1.000	0.351	0.436

C2. Tests for different solutions for vibration damping

Tests	X axis	Y axis	Z axis
HM	1.84	3.07	0.85
Rubber	1.79	2.76	0.84
Silicone	2.18	2.44	0.94
Dense Foam	2.21	2.75	1.00
Light Foam	2.21	2.87	1.20
WRIs	0.06	0.14	0.67

C3. Duro Inertial isolation

Tests	X axis	Y axis	Z axis
HM	4.15	3.28	2.49
45°	0.72	0.85	0.83
0° + 90°	0.66	1.48	0.98